

An empirical model for wind-generated ocean noise

John A. Hildebrand, Kaitlin E. Frasier, Simone Baumann-Pickering, and Sean M. Wiggins

Citation: *The Journal of the Acoustical Society of America* **149**, 4516 (2021); doi: 10.1121/10.0005430

View online: <https://doi.org/10.1121/10.0005430>

View Table of Contents: <https://asa.scitation.org/toc/jas/149/6>

Published by the [Acoustical Society of America](#)

ARTICLES YOU MAY BE INTERESTED IN

[Characterizing underwater noise during rain at the northeast Pacific continental margin](#)

The Journal of the Acoustical Society of America **149**, 4579 (2021); <https://doi.org/10.1121/10.0005440>

[Low-frequency ocean ambient noise on the Chukchi Shelf in the changing Arctic](#)

The Journal of the Acoustical Society of America **149**, 4061 (2021); <https://doi.org/10.1121/10.0005135>

[A series approximation to the Kirchhoff integral for Gaussian and exponential roughness covariance functions](#)

The Journal of the Acoustical Society of America **149**, 4239 (2021); <https://doi.org/10.1121/10.0005282>

[Multi-sensor integration for an assessment of underwater radiated noise from common vessels in San Francisco Bay](#)

The Journal of the Acoustical Society of America **149**, 2451 (2021); <https://doi.org/10.1121/10.0003963>

[Seabed type and source parameters predictions using ship spectrograms in convolutional neural networks](#)

The Journal of the Acoustical Society of America **149**, 1198 (2021); <https://doi.org/10.1121/10.0003502>

[Using context to train time-domain echolocation click detectors](#)

The Journal of the Acoustical Society of America **149**, 3301 (2021); <https://doi.org/10.1121/10.0004992>



**Advance your science and career
as a member of the**

ACOUSTICAL SOCIETY OF AMERICA

LEARN MORE



An empirical model for wind-generated ocean noise

John A. Hildebrand,^{a)} Kaitlin E. Frasier,^{b)} Simone Baumann-Pickering,^{c)} and Sean M. Wiggins^{d)}

Marine Physical Laboratory of the Scripps Institution of Oceanography, University of California San Diego, La Jolla, California 92037, USA

ABSTRACT:

An empirical model for wind-generated underwater noise is presented that was developed using an extensive dataset of acoustic field recordings and a global wind model. These data encompass more than one hundred years of recording-time and capture high wind events, and were collected both on shallow continental shelves and in open ocean deep-water settings. The model aims to explicitly separate noise generated by wind-related sources from noise produced by anthropogenic sources. Two key wind-related sound-generating mechanisms considered are: surface wave and turbulence interactions, and bubble and bubble cloud oscillations. The model for wind-generated noise shows small frequency dependence (5 dB/decade) at low frequencies (10–100 Hz), and larger frequency dependence (~15 dB/decade) at higher frequencies (400 Hz–20 kHz). The relationship between noise level and wind speed is linear for low wind speeds (<3.3 m/s) and increases to a higher power law (two or three) at higher wind speeds, suggesting a transition between surface wave/turbulence and bubble source mechanisms. At the highest wind speeds (>15 m/s), noise levels begin to decrease at high frequencies (>10 kHz), likely due to interaction between bubbles and screening of noise radiation in the presence of high-density bubble clouds.

© 2021 Author(s). All article content, except where otherwise noted, is licensed under a Creative Commons Attribution (CC BY) license (<http://creativecommons.org/licenses/by/4.0/>). <https://doi.org/10.1121/10.0005430>

(Received 22 February 2021; revised 10 May 2021; accepted 1 June 2021; published online 24 June 2021)

[Editor: Stephen Paul Robinson]

Pages: 4516–4533

I. INTRODUCTION

When the winds blow above the sea, underwater noise may be created by a variety of mechanisms including wind-generated surface waves, the impact of water droplets, and the entrainment of air bubbles into the surface layer. For most locations in the world's oceans, wind-generated sound is the dominant source of underwater ambient noise (Knudsen *et al.*, 1948) over a broad range of frequencies (400 Hz–50 kHz). However, at low frequencies (5–400 Hz), anthropogenic noise from commercial shipping overtakes wind noise as the dominant source of ambient sound (Wenz, 1962; Ross, 1976; Hildebrand, 2009).

Extensive underwater sound recordings allow an empirical model of wind-generated noise to be developed. Autonomous recordings collected by our group encompass more than one hundred cumulative years of data and capture high wind events. They were collected both on shallow continental shelves and in open ocean deep-water settings. The data are broadband (100 kHz) and with instrumental noise levels low enough to measure contributions of wind noise up to ~20 kHz (Wiggins and Hildebrand, 2007). In the frequency band 400 Hz–20 kHz, wind-generated noise often dominates other sources, and a clear correlation is seen between wind speed and noise level. At lower frequencies

of 10–400 Hz, local wind speed and noise levels are rarely correlated, and care must be exercised to discern the impact of wind in the absence of other sources of underwater sound. The source mechanisms for wind-generated noise in the band 400 Hz–20 kHz appear to be surface wave and turbulence interactions at low wind speeds (<3.3 m/s) and bubble oscillations at higher wind speeds. The source mechanism for wind-generated low frequency noise (10–400 Hz) is uncertain. Wind-generated noise increases with wind speed, but only up to a point. At the highest wind speeds ($u > 15$ m/s), noise levels begin to decrease for frequencies > 10 kHz, owing to interaction between bubbles and screening of noise radiation in the presence of high-density bubble clouds.

II. BACKGROUND

A. Physics of underwater noise

Agitation of the sea surface due to the passage of wind is a major source of underwater ambient noise (Wilson, 1980). Interaction of the wind with the sea surface detaches water droplets which both impact the sea surface and entrap underwater bubbles to generate sound (Franz, 1959). Droplet impacts are particularly created when breaking waves occur at increasing wind speed. The character of the sound produced is related to the first impact by the droplet and by the formation and oscillation of an entrapped bubble beneath the surface (Pumphrey and Elmore, 1990; Gillot *et al.*, 2020). The sound impulse created by the first impact is related to the kinetic energy of the droplet, a function of

^{a)}Electronic mail: jahildebrand@ucsd.edu, ORCID: 0000-0002-5418-9799.

^{b)}ORCID: 0000-0002-2401-8569.

^{c)}ORCID: 0000-0002-3428-3577.

^{d)}ORCID: 0000-0002-9686-035X.

droplet size and impact speed. The sound spectra radiated by the droplet impact has been shown to cover a wide frequency band (~100 Hz–10 kHz; Franz, 1959). The probability of entrapment of an air bubble also depends upon the droplet size and speed at impact (Pumphrey and Elmore, 1990), with some regions of the velocity and droplet size-space more likely to produce bubble entrapment (regular entrainment), while other conditions may or may not result in bubble formation (irregular entrainment). With regards to noise production from entrapped bubbles there are two separate classes of models: those that consider the response of individual bubbles (Loewen and Melville, 1991) and those that consider the collective oscillations of bubble clouds (Prosperetti, 1988; Means and Heitmeyer, 2001; Tkalich and Chan, 2002). A power law of between two and four is predicted for noise dependence upon wind speed due to bubble oscillations (Evans et al., 1984; Kerman, 1984).

Under low-wind conditions where there may be few or no breaking waves to produce bubbles, individual bubble or bubble cloud models may not adequately explain the full bandwidth of observed noise (2 Hz–50 kHz). Under conditions without breaking waves, three additional mechanisms have been put forward (Kewley et al., 1990) to explain wind-generated noise as a function of wind speed and frequency: (1) wind turbulence (Wilson, 1979), (2) ocean surface wave interactions (Kibblewhite and Ewans, 1985; Webb, 1998), and (3) surface wave turbulence interactions (Yen and Perrone 1979). In the frequency band 10–200 Hz it has been estimated that noise generated by surface wave-turbulence interaction may be dominant over the other two mechanisms (Yen and Perrone, 1979; Carey and Browning, 1988), and that noise from surface wave turbulence interaction should be directly proportional to wind speed and decrease as $\sim 1/f^2$.

Models that calculate noise are based on placing many random sources near the sea surface and then summing their contributions (Kuperman and Ingenito, 1980). In these models, a plane of monopole noise sources is positioned at one-quarter wavelength depth beneath the surface, leading to a dipole radiation pattern that is maximum in the downward direction. Further models have been proposed that account for attenuation of noise by sea surface bubble clouds, based on the distribution of bubbles with wind speed (Weston, 1989). At frequencies above 8 kHz and wind speeds above 15 m/s it has been found experimentally that noise levels decrease with increasing wind speed, likely due to scattering and absorption of sound by near surface bubbles (Farmer and Lemon, 1984).

B. Underwater noise models

Empirical relationships for underwater noise have been developed with wind speed as the primary independent variable (Knudsen et al., 1948; Wenz, 1962; Wilson, 1983). The most general empirical models (Carey and Evans, 2011) represent noise power (N dB re: $\mu\text{Pa}^2/\text{Hz}$) as a function of

frequency (f), observation depth (d), and wind speed (u) as follows:

$$N(f, d, u) = O(f, d, u) + 20 * n(f, d, u) \log_{10}(u) - 10 * m(f, d, u) \log_{10}(f). \tag{1}$$

This model recognizes that there is an expected logarithmic dependence of noise on wind speed, with the parameter $20 * n(f, d, u)$ giving the slope of the dependence. A value of $n = 1$ gives noise intensity that varies as the square of the wind speed, which has an intuitive appeal since the wind stress on the sea surface should vary as the square of wind speed. The parameter $10 * m(f, d, u)$ gives the frequency dependence of the noise. Based on Knudsen et al. (1948) and others (Kerman, 1984; Ma et al., 2005), the expected value of m for frequencies above 1 kHz is $\sim 5/3$ to 2. For frequencies below 400 Hz, m has been found to be nearly zero, with some dependence on wind speed (Urlick, 1984; Carey and Evans, 2011).

The primary depth-dependence of the noise is expressed in the parameter $O(f, d, u)$. Noise generated at the sea surface will experience attenuation as it propagates to depth (Urlick, 1975; Short, 2005; Kurahashi and Gratta, 2008), and the attenuation becomes significant at high frequencies and for deep sensors. An expression for the attenuation of noise at depth d can be obtained by considering the noise level received on an omnidirectional hydrophone J_o as follows:

$$J_o(d) = \iint J_{\Omega}(\theta, \phi, d) d\Omega, \tag{2}$$

expressed as the sum over contributions from the directional source J_{Ω} of ambient noise intensity per unit solid angle emitted by sea surface noise sources such as bubbles. Assuming straight-line ray paths and no reflections from the bottom, this becomes

$$J_o(ad) = 2\pi J_{\infty} \int_0^{\pi/2} \cos \theta e^{-ad \sec \theta} \sin \theta d\theta, \tag{3}$$

where J_{∞} is the average intensity per unit solid angle radiated by a unit surface area, θ is the angle of the ray arriving at the hydrophone, and a is related to the sound absorption coefficient α (Ainslie and McColm, 1998) by $\alpha d = -10 \log(e^{-ad})$, assuming surface dipole sources (Short, 2005). The depth-dependent noise correction O then becomes

$$O(f, d) = 10 \log_{10} \left(\frac{J_o(ad)}{J_o(0)} \right), \tag{4}$$

which will strongly limit high frequency noise ($> \sim 40$ kHz) at great depth (~ 1000 m).

C. Wind models

There have been significant improvements over the past decade in the measurement and modeling of ocean wind

using remote sensing data (Bourassa *et al.*, 2019). Ocean surface wind speed can be measured by satellite using microwave radiometers and scatterometers. In the former, a radiative transfer model is used to calculate microwave emission from the ocean surface, as well as absorption and emission by the atmosphere (Meissner and Wentz, 2012). Radiometer sensors that can measure wind speed include the Special Sensor Microwave Imager (SSM/I), Special Sensor Microwave Imager Sounder (SSMIS), Tropical Rainfall Mission Microwave Imager (TMI), Global Precipitation Mission (GMI), Advance Microwave Scanning Radiometer (AMSR), and WindSat. Radar scatterometers capable of wind measurement include the Quik Scatterometer (QuikSCAT), Advanced Scatterometer (ASCAT), Advanced Microwave Scanning Radiometers (AMSR-E and AMSR2), and the Micro-Wave Radiation Imager (MWRI). The radiometer and scatterometer data are validated with *in situ* measurements, with agreement to within 0.8 m/s (Bourassa *et al.*, 2019). The largest concerns are contamination from rain, issues with calibration at very high wind speeds, and the lack of data near land and over sea ice.

Global models of the wind are constructed by combining satellite winds and *in situ* observations to produce a gridded dataset. One such model is the Cross-Calibrated Multi-Platform (CCMP) wind analysis that uses a variational analysis method that includes an intercalibration of satellite radiometers and a refined sea-surface emissivity model and radiative transfer function to derive surface winds (Atlas *et al.*, 2011; Wentz, 2016). The European Center for Medium-Range Weather Forecasts (ECMWF) Interim Reanalysis winds are used in the CCMP V2.0 as the initial estimate of the wind field. The CCMP model references all wind observations (satellite and *in situ*) to a height of 10 meters.

III. METHODS

A. Underwater sound dataset

A significant dataset of underwater sound has been collected by our lab over more than a decade using autonomous acoustic recorders (Wiggins and Hildebrand, 2012). Beginning in 2004, the High-frequency Acoustic Recording Package (HARP) data logger was developed to provide long-term (~1 year) and broadband (~100 kHz) recording capabilities for remote acoustic monitoring (Wiggins and Hildebrand, 2007). The HARP is configured as a seafloor or water-column autonomous mooring with internal data storage and battery power. These instruments have been used for a range of studies of ambient noise and anthropogenic sound sources such as ships and airguns (McKenna *et al.*, 2012; Roth *et al.*, 2012; Wiggins *et al.*, 2016; Gassmann *et al.*, 2017).

A dataset of 291 instrument deployments with 50 455 days (138 years) of acoustic data collection between 2007 and 2019 are examined in this study (Appendix, Table V). Data were collected at 72 unique sites that cover a broad range of latitude and depth, including areas with seasonally strong winds such as the Gulf of Alaska, Western Atlantic/

Gulf of Mexico, and Southern Ocean (Fig. 1). In almost all cases, the instrument package was placed on the seafloor and the hydrophone was positioned 10–30 m above the instrument package.

Calibrated hydrophones and recording electronics are used in the HARP to determine accurate received sound pressure levels. All hydrophone sensors are lab-calibrated before deployment and at the end of service life, and representative hydrophones are full system calibrated at the U.S. Navy’s transducer evaluation center, TRANSDEC, in San Diego, CA. The design of the HARP hydrophone employed piezoelectric ceramic sensors, either as single or as multiple elements, to cover the frequency band from 10 Hz–100 kHz (Table VI). When multiple elements were employed, one group was optimized for the low-frequency band (10 Hz–2 kHz or 20 kHz) using a bundle of six individual elements (Benthos AQ-1) and the other was optimized for the high frequency band using a single spherical element (typically ITC 1042). Changes in the HARP hydrophone design over the period of this study were primarily in the amount of gain applied to the high frequency band and the location of the crossover between the high and low frequency sensor bands. For the purpose of this study, we recognize five distinct hydrophone designs that are numerically designated by their pre-amplifier numbers (Table VI). The acoustic data were sampled at 200 kHz (16-bit resolution) and processed into 100-Hz bin-width, 5-s duration spectral averages for the band 100 Hz–100 kHz, and after decimating by a factor of 5, into 10 Hz bin-width spectral averages for the band 10 Hz–1000 Hz. Times when the instrument was writing to its internal disk storage were eliminated from these spectral averages. These 5-s spectral averages were further combined to obtain an hourly estimate of the noise spectra over 10 Hz–100 kHz.

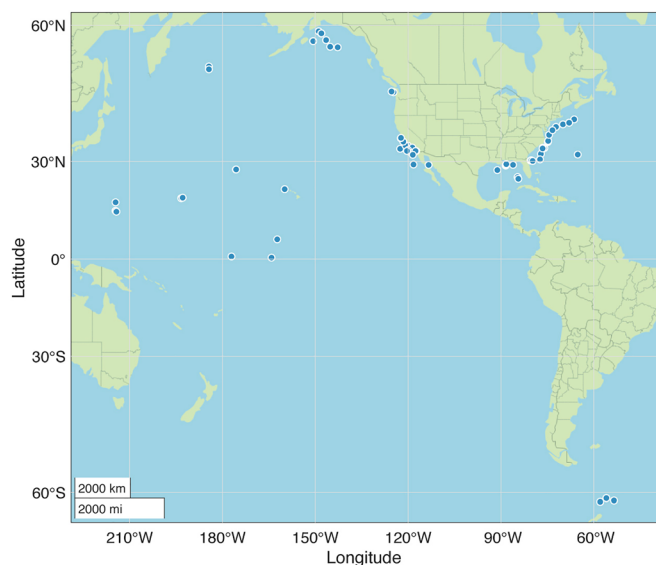


FIG. 1. (Color online) Locations of acoustic recordings used in this analysis. See Appendix, Table V, for listing of deployment locations, dates, and seafloor depths. Sensor depths are 10–30 m above the seafloor.

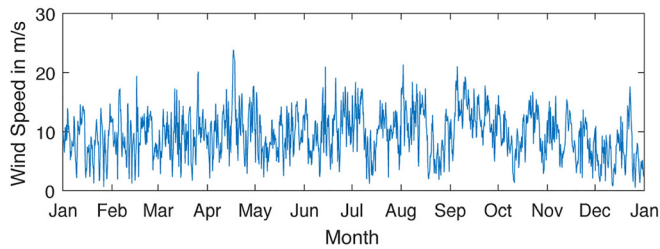


FIG. 2. (Color online) Wind speed from the CCMP v2 model for the year 2016 at a site in the Southern Ocean (latitude 61-22.5 S, longitude 53-22.5 W).

B. Wind data

The CCMP v2 model was used to estimate the wind speed at 10 m altitude above each HARP deployment location simultaneous with the acoustic recording (Atlas *et al.*, 2011; Wentz, 2016). The CCMP v2 model provides estimates on a 0.25-degree spatial resolution grid with 6-h time resolution. Wind data were used from the closest grid point to the deployment, no more than 0.125-degree (14 km) distant. The wind data were interpolated to a 1-h resolution and combined with the 1-h average of the acoustic data (Fig. 2). The lack of temporal resolution in the wind model precluded incorporating the impact of short-term high-speed wind gusts into the modeling effort. For each deployment, plots were made to assess the correlation of sound levels and wind speed at various frequencies (Fig. 3), and deployments with little or no correlation were removed from the analysis. The Southern Ocean site shown in Fig. 3 is particularly illustrative of the contributions of wind because it is remote from major shipping lanes. Sites that were nearby islands or coastlines with high topographic relief (e.g., Kona, HI) showed poor correlation between the predicted wind and the sound level, presumably due to lack of spatial resolution in

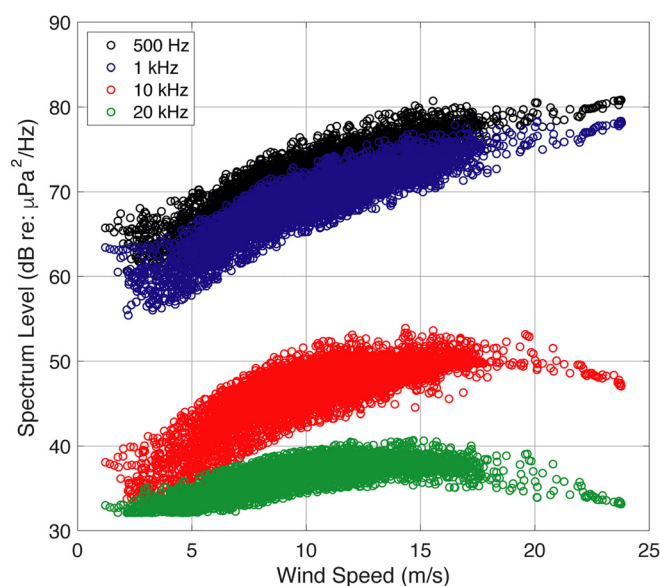


FIG. 3. (Color online) Sound level versus wind speed at four frequencies (0.5, 1, 10, 20 kHz) in the Southern Ocean (Site EIE, 61-15.112 S, 53-29.006 W, 1033 m) from February 3 to December 2, 2016.

the global wind model. Outliers in the wind speed versus noise level plots were removed using a spline fit to the data, eliminating data points with greater than 95% standard deviation from the mean of the fit.

A comparison between the sound data and the wind data at each site was conducted by segmenting the wind data into speed categories corresponding to Beaufort sea-state numbers (WMO, 1970) as given in Table I, and plotting noise versus broadband frequency for each Beaufort number (Fig. 4). These provide an assessment of the shape of the noise spectra versus frequency and allow determination of which portions of the spectral band are wind-related. There is a high correlation between wind speed and noise level in the frequency band 300 Hz–20 kHz. The noise level is flat with frequency, and independent of wind speed for frequencies above ~20 kHz, suggesting that these data are set by instrumental electronic noise. At the lowest frequencies (<100 Hz) wind speed dependence is only observed by careful selection of data for high wind events, in areas secluded from distant shipping noise, and after removing periods of local anthropogenic noise. For this dataset, these conditions only occurred for Southern Ocean sites, and for sites that were sheltered from long-range propagation by local bathymetry such as in the California Borderlands and in the Gulf of California.

An alternative approach to understanding the relationship between the noise and wind data is to plot the noise level versus wind speed at a fixed frequency (Fig. 5). At low frequencies (<100 Hz), these plots show little correlation between noise level and wind speed, whereas for frequencies of 300 Hz–20 kHz an approximately linear relationship is observed for wind speed scaled as \log_{10} . A regression analysis for wind speeds $u > 5$ m/s was calculated to provide an estimate of the wind dependent parameter $n(f,d,u)$ from Eq. (1) (red lines in Fig. 5). A change in slope is often observed for wind speed $u < 5$ m/s and a lower value of $n(f,d,u)$ is observed, related to the lack of breaking waves (Evans *et al.*, 1984; Kerman, 1984). There is also a change of slope for the highest frequencies (10 and 20 kHz) at the highest wind speeds, likely related to interference between bubbles (Farmer and Lemon, 1984).

TABLE I. Wind speed equivalent of Beaufort numbers. WMO code 11001946 international equivalents in m/s at 10 m altitude (WMO, 1970).

Beaufort	Minimum	Average	Maximum
0	0	0	0.2
1	0.3	0.9	1.5
2	1.6	2.4	3.3
3	3.4	4.4	5.4
4	5.5	6.7	7.9
5	8.0	9.3	10.7
6	10.8	12.3	13.8
7	13.9	15.5	17.1
8	17.2	18.9	20.7
9	20.8	22.6	24.4
10	24.5	26.4	28.4
11	28.5	30.5	32.6

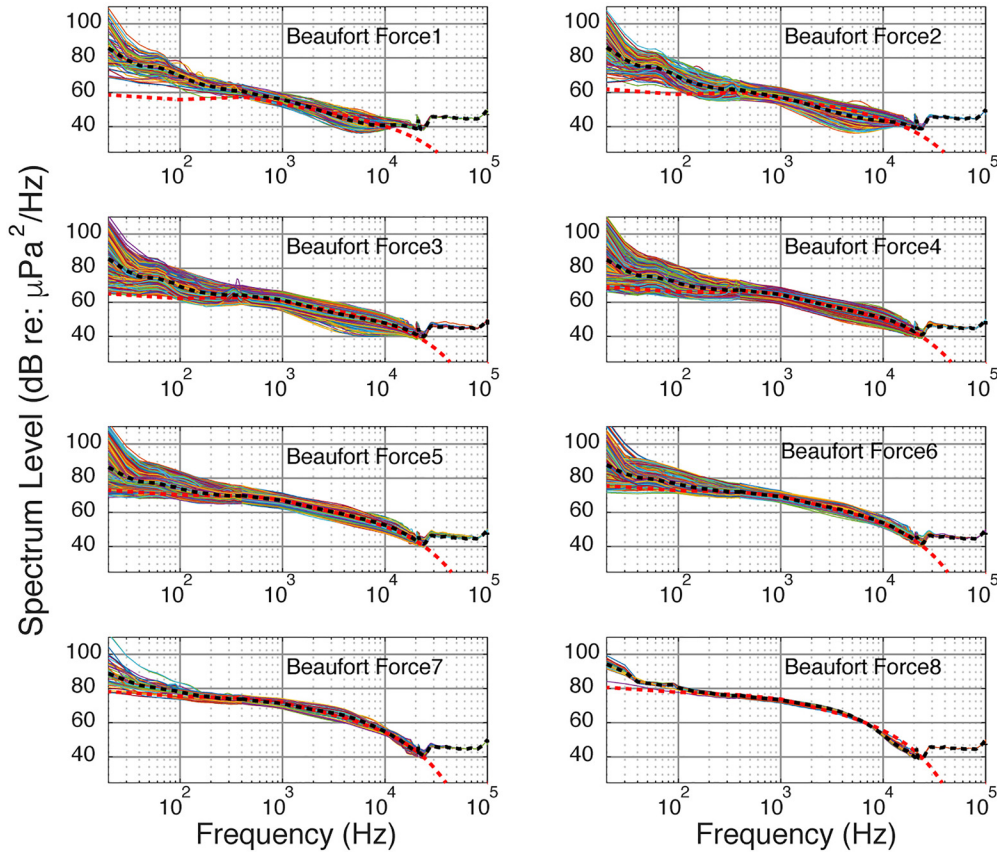


FIG. 4. (Color online) Noise spectrum levels grouped by Beaufort force in the Southern Ocean (site EIE as in Fig. 3). Dashed black line is deployment average, other colored lines are 1-h averages. Dashed red line is ocean noise model. Note that all spectra are electronic noise dominated above ~ 20 kHz.

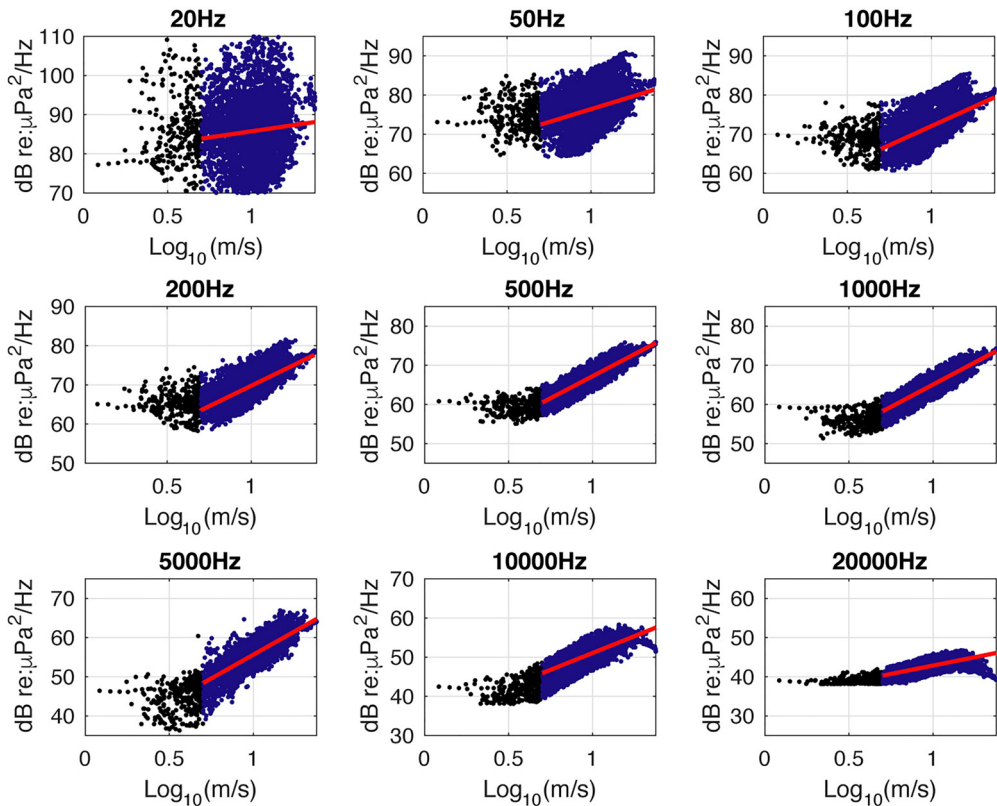


FIG. 5. (Color online) Noise spectrum levels for a selection of frequencies (20, 50, 100, 200, 500, 1000, 5000, 10 000, 20 000 Hz) plotted as a function of wind speed for the Southern Ocean (site EIE as in Fig. 3). Red line is linear regression for data above $\log_{10}(5 \text{ m/s}) = 0.7$ (blue datapoints).

C. Model

A model for wind-generated underwater noise was created to match the observed wind and sound data described above following the form of Eq. (1). Starting parameters for the model, especially the wind dependence $n(f,d,u)$ and the frequency dependence $m(f,d,u)$ were obtained from previously published studies (Piggott, 1964; Perrone, 1969; Burgess and Kewley, 1983; Urick, 1984; Kewley et al., 1990; Marrett and Chapman, 1990; Chapman and Cornish, 1993; Ma et al., 2005; McDonald et al., 2008; Carey and Evans, 2011; Reeder et al., 2011). The goodness of fit between the model and the observation data was determined as a function of sensor depth, binning the observation data into 200 m intervals. Where the model systematically deviated from the trends of the observation data, the parameters $n(f,d,u)$, $m(f,d,u)$, and $O(f,d,u)$, were adjusted to allow for better agreement. The goal of these adjustments was to keep the average mis-match between the model and the observation data under ~1 dB for all depth bins. The volume of the dataset, the large numbers of free-parameters in the model, and the need to exclude data that were contaminated by anthropogenic noise sources, precluded an automated parameter estimation. Every effort was made to keep the size of both linear and non-linear parameters in the model to a minimum and to test for sensitivity to individual parameters.

IV. RESULTS

A. Wind dependence parameter

The wind dependence parameter $n(f,d,u)$ is obtained for each dataset from linear regression of noise versus wind speed (Fig. 5). The values of $n(f,d,u)$ for the entire dataset are plotted as a function of frequency in Fig. 6 and median numerical values and linear regression goodness of fit are presented in Table II. At low frequencies (<100 Hz) factors other than the wind significantly contribute to underwater ambient noise, resulting in low correlation and wind dependence parameter estimates of 0.2–0.5 (Table II). For frequencies in the range 200 Hz–10 kHz, the wind dependence parameters are in the range $n = 0.9$ –1.2, near the expected value of 1.0 due to wind stress on the ocean surface (albeit with extended tails for the distribution at 200 and 500 Hz, suggesting some vessel traffic contamination). At the highest frequencies that can be discerned above instrumental noise, 20–30 kHz, an alternate phenomenon is manifest, with wind dependence parameters of ~0.5. Indeed, at these frequencies, a simple linear regression does not represent the curvilinear relationship between wind speed and noise, as illustrated in Fig. 5.

To account for the depth and frequency dependence observed, additional factors ($nfac1$, $nfacnl$, $nfacf$) were introduced into the wind parameter $n(f,d,u)$ as follows:

$$n(f, d, u) = n - \left(\frac{d}{nfac1} + An * \exp\left(-\frac{d}{nfacnl}\right) \right) * Bn * n * (freq - nfacf)/fmax, \tag{5}$$

where d is depth, $nfac1$ is a linear depth parameter ($nfac1 = 1000$ m), $nfacnl$ is a non-linear depth parameter ($nfacnl = 400$ m), $nfacf$ is the frequency at which the non-linear depth parameter begins, and An , Bn are constants (Table III). The impact of the linear and non-linear depth terms is to decrease n increasingly with both depth and above frequency $nfacf$. Wind speed dependence was also introduced into the wind parameter $n(f,d,u)$. At the lowest Beaufort force (numbers 1 and 2) it was determined that $n = 0.5$, while $n = 1.0$ at Beaufort force 3, and $n \rightarrow 1.5$ for higher Beaufort force numbers.

B. Frequency dependence parameter

The frequency dependence parameter $m(f,d,u)$ is obtained from plotting noise level versus frequency, binned by Beaufort number, as in Fig. 4. At low frequencies (<100 Hz), noise levels at high wind speed sometimes exceed those of anthropogenic noise sources (e.g., commercial shipping). However, at low wind speeds, the only way to observe wind noise is to select for locations that are distant or shielded from ship noise (McDonald et al., 2008; Reeder et al., 2011) and to select for periods of time that exclude local ships and periods of high instrumental noise from flow or strum (see lowest noise levels in Fig. 4). The frequency parameter $m(f,d,u)$ was found to be -0.5 to $+0.3$ for frequencies below 400 Hz. At higher frequencies (1–20 kHz) $m(f,d,u)$ is in the range from -1.0 to -1.5 .

To account for the depth dependence of $m(f,d,u)$ additional factors ($mfac1$, $mfacf$) were introduced as follows:

$$m(f, d) = m - \left(1 - \frac{d}{mfac1} \right) * Am * \frac{(mfacf - freq)}{fmax}, \tag{6}$$

where d is depth, $mfac1$ is a linear depth parameter ($mfac1 = 1000$ m), $mfacf$ is the frequency at which the non-linear depth parameter begins ($mfacf = 15$ kHz), and Am is a constant ($A = 2.5$ dB). In practice, the impact of this term is to decrease $m(f,d,u)$ from -1.5 to -2.0 for frequencies above 10 kHz and at shallow depths (<500 m).

C. Offset parameter

The offset parameter $O(f,d,u)$ adjusts the noise model to allow for its continuity over frequency and wind speed with changes in the wind $n(f,d,u)$ and frequency $m(f,d,u)$ parameters. It also allows explicit adjustment for depth-dependent attenuation, as described earlier using the model of Short (2005). An additional depth-dependent term was found to be needed as follows:

$$O(d) = Ao * \exp\left(-\frac{d}{Bo}\right), \tag{7}$$

where d is depth, Ao is an amplitude in dB ($Ao = 2.8$ dB), and Bo is the depth for 1/e decrease in influence ($Bo = 600$ m). This term partially accounts for bottom interaction, which was

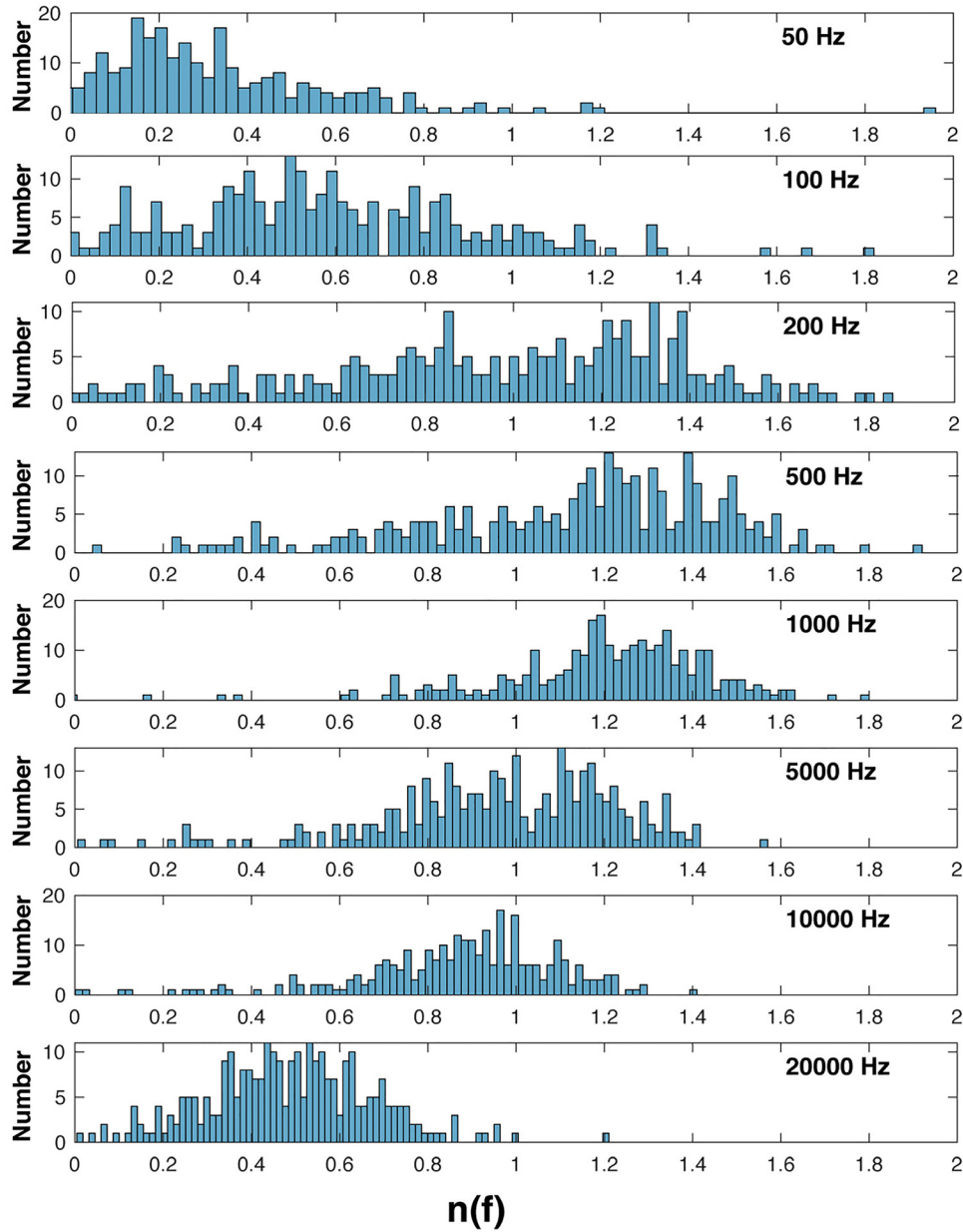


FIG. 6. (Color online) Histogram counting the number of deployments with wind dependence parameter $n(f)$ plotted by frequency (50 Hz–20 kHz) for all deployments (291 total).

TABLE II. Wind dependence parameter $n(f, d, u)$ median and mean goodness of fit (R^2). Number of deployments (n) is indicated for each depth range, for a total of 291 deployments analyzed.

Frequency	Median ($n = 291$)	Goodness of fit (R^2)	<200 m ($n = 15$)	400 m ($n = 14$)	600 m ($n = 23$)	800 m ($n = 38$)	1000 m ($n = 84$)	1200 m ($n = 67$)	1400 m ($n = 50$)
50 Hz	0.22	0.05	0.27	0.28	0.18	0.26	0.29	0.20	0.21
100 Hz	0.50	0.34	0.39	0.79	0.51	0.43	0.50	0.50	0.50
200 Hz	1.00	0.51	0.66	1.18	0.66	0.91	0.93	0.96	1.00
500 Hz	1.20	0.78	0.74	1.24	0.97	1.09	1.15	1.17	1.20
1000 Hz	1.22	0.77	0.96	1.31	1.13	1.19	1.21	1.24	1.18
5000 Hz	0.99	0.66	1.11	1.16	0.85	0.85	1.04	0.95	0.86
10000 Hz	0.90	0.60	0.95	1.07	0.82	0.76	0.94	0.86	0.80
20000 Hz	0.49	0.45	0.59	0.76	0.51	0.45	0.54	0.44	0.35

TABLE III. Wind parameters $nfacf$, An , and Bn by Beaufort force. See Eq. (5).

Beaufort	4	5	6	7	8	9	10	11
$nfacf$ (Hz)	20 000	20 000	10 000	6200	4100	4100	4100	4100
An (dB)	0.04	0.08	0.17	0.24	0.6	1.0	1.6	1.8
Bn (dB)	0.3	0.3	0.7	1.2	1.8	2.2	2.5	2.7

neglected in the Short (2005) analysis, adding about 2 dB at 200 m depth, and 1 dB at 600 m.

D. Hydrophone calibration

Segregating the dataset by hydrophone type allowed testing for systematic deviations from their laboratory calibrations. The average misfit between the model and data for each hydrophone type revealed small (0–4 dB) deviations from the laboratory calibrations. Figure 7 shows the average transfer-function correction by hydrophone type. Most of the deviations from laboratory transfer functions occur near the crossover frequency between lower and upper frequency sensors. For the 500 and 600 series hydrophones, at the crossover frequency near 3–5 kHz, deviations of 2–3 dB are observed. For the 700 series hydrophone, deviation is seen at the crossover frequency near 20 kHz, and there also appears to be a linear correction to the gain with frequency, with an amplitude of about +4 dB at 20 kHz and –2 dB at 300 Hz. Since these corrections are systematic by hydrophone type, they are applied as a correction to the dataset.

E. Wind-generated noise model

The wind-generated underwater noise model is plotted as a function of frequency for a set of wind speeds or sea-states (Knudsen *et al.*, 1948) as shown for the models in Fig. 8 (left) calculated for three sensor depths (100, 500, and

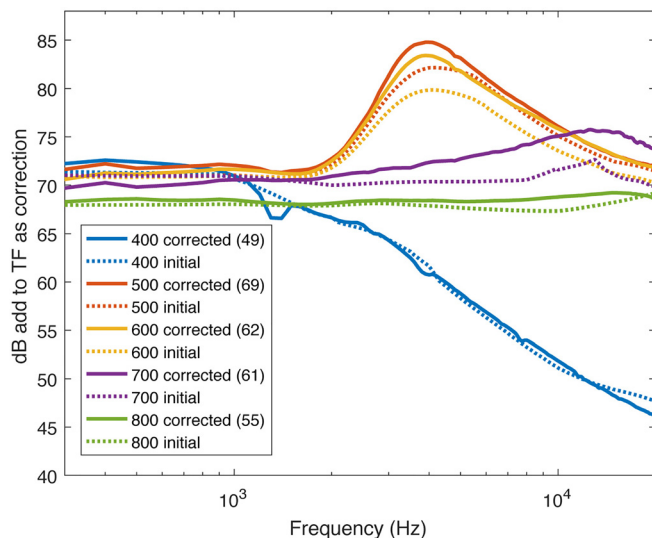


FIG. 7. (Color online) Hydrophone transfer functions by series (400, 500, 600, 700, 800) with the number of hydrophones used from each series in parentheses. Dotted line is initial estimate, solid line is corrected using the difference between the study dataset and the wind model.

1000 m). At low wind speed (Beaufort 1–4) noise levels decline from 10 to 100 Hz, and then increase from 100 to 400 Hz to a local maximum at 400 Hz, before falling with slopes of $\sim m = 1-1.5$ for frequencies above 1 kHz. For higher wind speeds (Beaufort 5–11) the local noise maxima at 400 Hz disappears and noise decreases uniformly for frequencies between 10 Hz and 1 kHz. At high wind speeds (Beaufort 8–11) and high frequencies (>10 kHz), a striking feature of the model is the crossover of noise curves producing lower noise levels at higher wind speeds for these conditions. For models at depth (1000 m), attenuation becomes a factor at frequencies >10 kHz, resulting in low noise levels independent of wind speeds. The parameters used to calculate these models [$n(f,d,u)$, $m(f,d,u)$] and $O(f,d,u)$, are given as a function of frequency and Beaufort force in Fig. 9.

The goodness-of-fit for the model is calculated as an average for all the deployments in each 200 m depth interval (Fig. 10). All depth interval averages fit the noise model to within ± 1 dB across the frequency band 200 Hz–20 kHz, except for the shallow interval 0–200 m. When all the deployments are averaged together, the misfit is <0.25 dB. The 0–200 m depth interval shows systematic deviations of $\sim 1-1.5$ dB with frequency, presumed to be due to bottom interactions and shallow water propagation effects (Ingenito and Wolf, 1989) that create constructive and destructive interference that is not included in the model. Figure 4 plots the model prediction (dashed red line) against the data collected at the Southern Ocean site. The model and Southern Ocean average noise data (dashed black line) agree well in the frequency range 200 Hz–20 kHz, but deviate for frequencies >20 kHz due to instrumental electronic noise. Below 200 Hz, the model and data agree only during the lowest noise periods, presumably due to the influence of residual anthropogenic sources and instrumental noise from periods of high flow and strum.

V. DISCUSSION

A comparison of the present model to previous noise models and observations is given in Table IV. The previous studies are divided into shallow (< 200 m) and deep-water (~ 1000 m) with the present model calculated at 100 and 1000 m for comparison. As noted previously by Urick (1984) the observational data are inconsistent between published sources, presumably due to differences in local conditions as well as system calibrations and data analysis methods. For the shallow water data, the pioneering study of wind noise by Knudsen *et al.* (1948) has comparable sound levels to the present model [root-mean-square (rms) difference of 1.6 dB], but the non-linearity of noise with wind speed suggested by Knudsen *et al.* (1948) between Beaufort Force 2–5 is not substantiated by the present model. The wind speed curves of Wenz (1962), adjusted for shallow water, are consistent with both the Knudsen *et al.* (1948) model and the present model, except at the lowest wind speeds (Beaufort force 1). The data of Piggott (1964) and Wille and Geyer (1984) are both higher in level (5.5 and

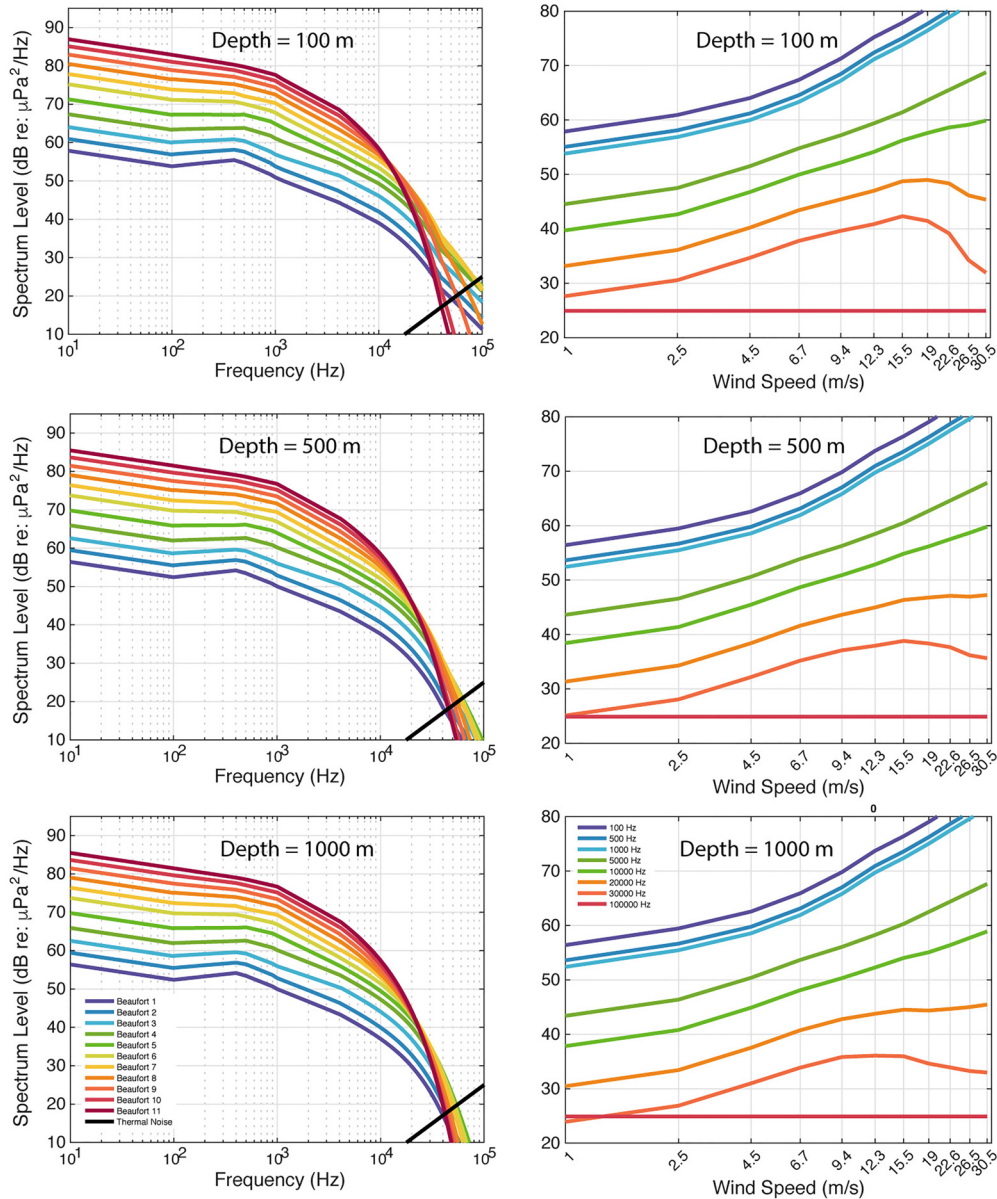


FIG. 8. (Color online) Model for wind-generated noise as a function of (left) frequency and (right) wind speed calculated for sensors at depths 100 m (top), 500 m (middle), and 1000 m (bottom). Legend gives Beaufort force numbers from 1 to 11 (colors) and black line is level of thermal noise.

2.9 dB rms, respectively) than the present study. The more recent shallow water studies of [Ma et al. \(2005\)](#) and [Nystuen et al. \(2010\)](#) are in good agreement with the present model, except for a lower than expected value at low wind speed (Beaufort force 2).

For deep water, the present model was calculated at a sensor depth of 1000 m for comparison with previous studies. Following installation of US Navy surveillance arrays beginning in the 1950s, studies were conducted to document the wind speed dependence of ambient noise in deep water. During commissioning of these arrays in the Atlantic, [Ross \(1954\)](#) produced a generalized ambient noise spectra (see the supplementary material Fig. 1)¹ that is largely in agreement with the present model (1.1 dB rms difference). Subsequent studies conducted by [Wenz \(1962\)](#) and [Perrone \(1969\)](#) are lower than the present model (4.2 and 5.0 dB rms,

respectively) especially at the low (Beaufort force 1) and high (Beaufort force 8) ends of the wind spectrum. This may be the result of a lack of accurate wind speed data, and/or use of *Atlas of Climatic Charts of the Oceans* or similar to approximate wind speed; presumably good estimates were available for average wind speeds, but poor estimates for periods of very low and very high winds. The idealized ambient noise spectra of [Urlick \(1984\)](#), based on both a literature review and expert knowledge of spectral behavior of noise sources, is consistent with the present model (1.4 dB rms difference), as are the measurements of [Cato \(1976\)](#) made in waters near Australia, and the measurements of [Reeder et al. \(2011\)](#) made in the Bahamas.

Several features of the empirical noise model are noteworthy and provide insight into possible source mechanisms and areas where more understanding is needed. The first

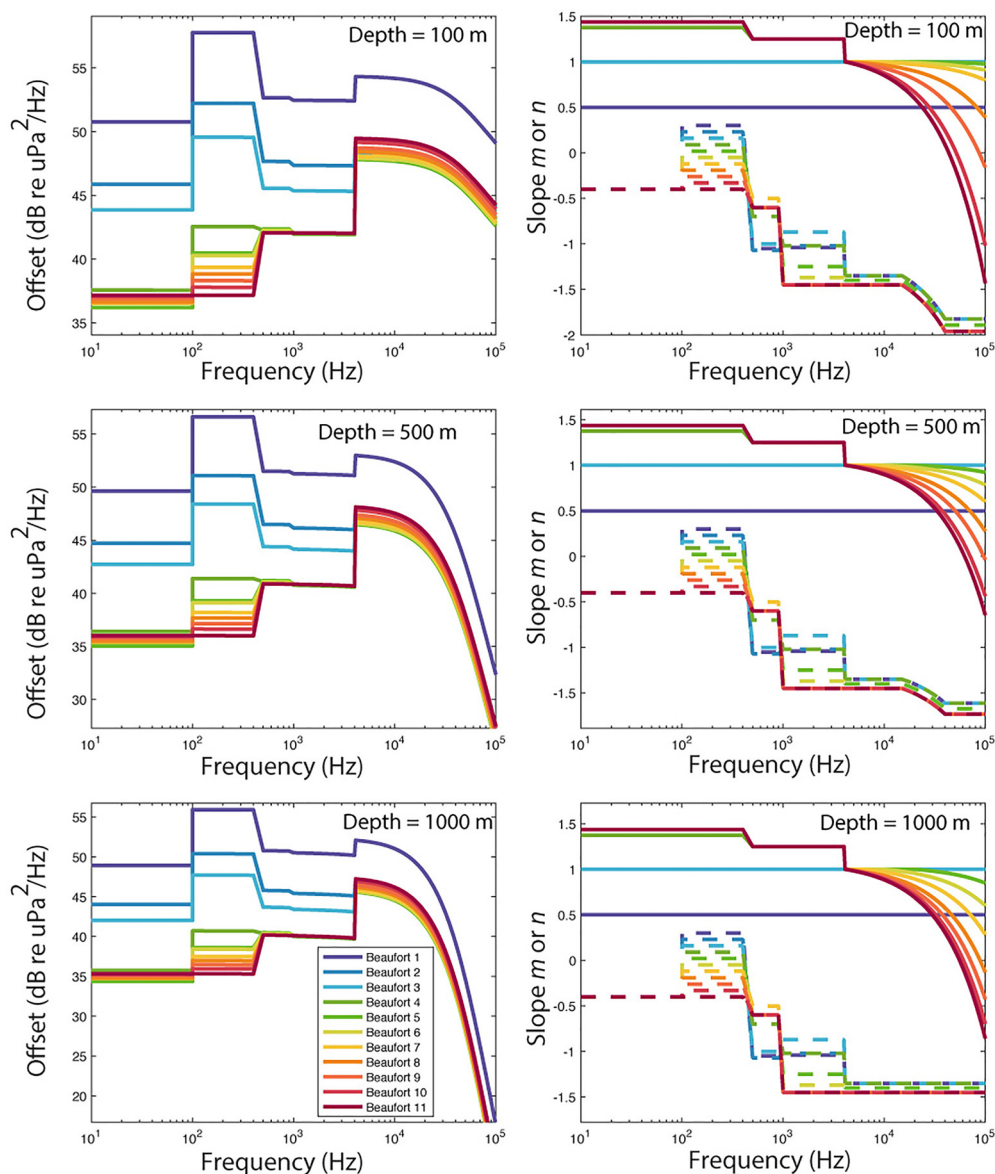


FIG. 9. (Color online) Parameters for wind noise model, offset (left), wind dependence parameter n (right solid line) and frequency parameter m (right dashed line) for depths 100, 500, and 1000 m. Legend gives Beaufort force (color).

point is that the model at low frequency (10–100 Hz) separates wind contributions to ambient noise from those of anthropogenic sources such as commercial shipping. For most locations, omni-directional ambient noise at low frequencies is dominated by the sum of many distant ships, or in some locations seismic surveys (Wiggins *et al.*, 2016), and the contribution of wind is not easily discernable. Many efforts to separate wind noise from anthropogenic noise have been based on the use of an acoustic array to separate distant (horizontally propagating) from local (vertically propagating) sources (Kewley *et al.*, 1990; Chapman and Cornish, 1993; Farrokhrooz *et al.*, 2017). Instead, the model we present is derived from omni-directional hydrophones placed at locations sheltered from ship noise at low wind speeds (McDonald *et al.*, 2008; Reeder *et al.*, 2011), and at times of extreme wind speed when ship noise may no longer be dominant. Sites in the southern hemisphere are

particularly helpful in minimizing the presence of distant shipping noise.

The low frequency portion of the model presented here has frequency dependence of about 5 dB/decade ($m = -0.5$) or less for noise below 400 Hz. This is in contrast to the slopes of ~ 15 dB/decade ($m = -1.5$) seen above 1 kHz in the model. Both bubble cloud and surface wave–turbulence source mechanisms (Yen and Perrone, 1979) have a presumed 20 dB/decade frequency dependence ($1/f^2$). The portion of the noise model above 1 kHz is roughly in accord with this slope, but the noise model below 400 Hz is not, pointing out an incomplete understanding of what is the source of low frequency wind-related noise in the absence of shipping. Along these lines, the frequency band between 100 and 400 Hz may be a zone of transition between two different noise generation mechanisms. The presence of flow noise and cable strum is a possibility at low frequencies.

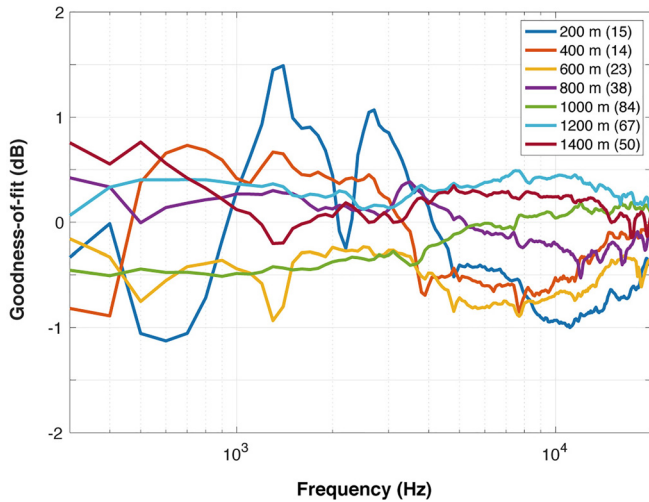


FIG. 10. (Color online) Goodness-of-fit for the noise model by sensor depth in 200 m intervals. Legend gives color for each depth interval (e.g., 0–200 m dark blue) and the number of deployments for that depth range (in parenthesis).

Care has been taken in the hydrophone design and cable attachment to minimize these effects, but they are difficult to protect against during periods of high flow. However, the discontinuity in low frequency, low wind-speed noise makes it less than expected, so additional hydrophone flow and strum noise would not explain the difference.

For low wind speeds ($u < 3.3$ m/s) noise levels and wind speed have a directly linear relationship ($n = 0.5$). Whereas for higher wind speeds ($u > 5.5$ m/s), the relationship is a power law of two or three ($n = 1.0$ to 1.5). This suggests that there is a transition between a source mechanism of surface wave-turbulence interactions at low wind speeds, with a linear dependence on wind speed, and the presence of breaking waves and their associated bubble formation at higher wind speeds, with a higher power law relationship.

TABLE IV. Comparison of 1 kHz wind-noise spectrum level (dB re: $\mu\text{Pa}^2/\text{Hz}$) between the model presented here and that of previous ocean noise models and data. The values for previous studies are given with 0.5 dB precision due to the difficulty of estimation from published graphics. The rms (dB) difference between the present model and the published study is given in the right-hand column, comparing the model with the sensor depth at 100 m and shallow water studies, and the model at 1000 m and deep water studies.

Beaufort Force	Depth	1	2	3	4	5	6	7	8	rms
This Model	100 m	52.5	55.3	58.4	62.6	66.4	69.3	71.8	74.0	
Knudsen (1948)	Shallow	51.0	55.5	61.5	64.5	66.5		71.0		1.6
Wenz (1962)	Shallow	47.5	55.5	60.5		67.5			73.5	2.5
Piggott (1964)	Shallow	50.0	60.0	65.0		73.0			80.0	5.5
Wille and Geyer (1984)	Shallow			62.5	67.0	69.0	71.5	73.0	75.0	2.9
Ma et al. (2005)	Shallow				61.0					1.6
Nystuen (2010)	Shallow		49.0	59.0	63.0	66.0	68.0	70.5		2.7
This Model	1000 m	50.5	53.4	56.5	60.7	64.4	67.4	69.9	72.1	
Ross (1954)	Deep	50.0	54.0	58.0	61.0	64.0		68.0		1.1
Wenz (1962)	Deep	42.5	50.5	55.5		62.5			68.5	4.2
Perrone (1969)	Deep		50.0	52.0		60.0			65.0	5.0
Reeder et al. (2011)	Deep			55.5	60.0	64.0				0.7
Wenz (1962)	Average	45.0	53.0	58.0		65.0			71.0	2.6
Urlick (1984)	Various		53.0	58.5		66.0			71.0	1.4
Cato (1976)	Various	54.0			61.0	65.0				2.0

Another feature of the noise model is that at frequencies > 10 kHz and for Beaufort number > 7 ($u > 17$ m/s), noise levels diminish with increasing wind speed, as shown for the Southern Ocean data in Fig. 3. Given that bubble cloud oscillations appear to be the dominant source mechanisms under these conditions, one possibility is that strongly energetic winds inject greater volumes of bubbles and to a greater depth, such that there may be interference between bubbles either in limiting additional sound generation and/or in limiting propagation of the generated sound from the near surface source region. It has been previously suggested that the acoustic radiation from newly formed bubbles can be both scattered and absorbed by previously entrained bubbles (Farmer and Lemon, 1984; Updegraff and Anderson, 1991).

Despite the smooth appearance of the noise model in both frequency and in wind speed (Fig. 8), the parameters used to generate it are discontinuous in both variables (Fig. 9). This is a result of the piecewise construction of the model, resulting in discontinuities in the wind dependence and frequency dependence parameters, and associated discontinuities in the offset parameter. A full inversion for these parameters may allow for the development of both a smooth model and a smooth set of model parameters, and help to discover more subtle features of the dataset than possible with the current approach. Also, despite the large volume of data that went into the current model, it will be possible to validate and update the model with more recent wind and acoustic data as they become available.

VI. CONCLUSION

A large underwater noise dataset and global wind model were combined to produce an empirical model for the dependence of underwater noise on local winds. The model explicitly separates noise generated by sources related to the wind from anthropogenic sources of underwater sound. The

model for wind-generated noise shows small (5 dB/decade) frequency dependence at low frequencies (10–100 Hz), and larger (~15 dB/decade) frequency dependence at higher frequencies (400 Hz–20 kHz). The relation between noise level and wind speed is linear for low wind speeds ($u < 5$ m/s) and increases to a higher power law (two or three) at higher wind speeds, suggesting a transition between the presence of breaking waves and their associated bubble formation. At the highest wind speeds ($u > 15$ m/s), noise levels begin to decrease at high frequencies (>10 kHz) due to interaction between bubbles and screening of noise radiation in the presence of high-density bubble clouds.

ACKNOWLEDGMENTS

The authors acknowledge the long-term support of a large number of agencies and individuals in the collection of these acoustic data including, the Chief of Naval Operations N45 (Frank Stone, Ernie Young, and Anu Kumar), Office of Naval Research (Robert Gisiner, Michael Weise, and Robert Headrick), U.S. Pacific Fleet

(Chip Johnson, Jessica Brevdik, and Christiana Salles), U.S. Atlantic Fleet (Gene Nissen and Joel Bell), Duke University (Andy Read), OST-NOAA (Jason Gedamke), PIFSC-NOAA (Erin Oleson and Ann Allen), NEFSC-NOAA (Sophie Van Parijs and Danielle Cholewiak), SEFSC-NOAA (Lance Garrison and Melissa Soldevilla), University of South Florida-GOMRI/CIMAGE (Steve Murawski and Sherryl Gilbert), Channel Islands NMS (Chris Mobley), UCSB-BON (Robert Miller), Pacific Life Foundation (Bob Haskell and Tennyson Oyler), UABCS (Jorge Urban), Oceanides Conservación y Desarrollo Marino (Gustavo Cárdenas-Hinojosa), and Fundación Cethus (Miguel Iñiguez and Mariana Melcon). We thank Marie Roch, Ana Širović, Josh Jones, Ethan Roth, Hannah Basset, Chris Garsha, Ryan Griswold, Brent Hurley, Bruce Thayre, John Hurwitz, Ally Rice, Jennifer Trickey, Macey Rafter, Alba Solsona Berga, Erin O’Neill, and Beverly Kennedy for coordinating instrument deployment, recovery, and data processing. A final thanks to Don Ross for his guidance and pioneering work on ocean noise.

APPENDIX

See Tables V and VI for acoustic recorder deployment metadata and hydrophone specifications, respectively.

TABLE V. Acoustic recorder deployment metadata including hydrophone number, latitude, longitude, water depth, data start date, data end date, and recording duration in days.

Data_ID	Hyd number	Latitude	Longitude	Depth (m)	Data_start	Data_end	Rec_Dur (days)
Aleut_BD_02	600	52-38.000 N	175-37.990 E	783	8/27/2010	5/26/2011	273
Aleut_BD_03	600	52-04.560 N	175-38.390 E	777	5/31/2011	8/26/2012	454
Antarc_EIE_01	729	61-15.112 S	53-29.006 W	1033	2/3/2016	12/2/2016	302
Antarc_EL_01	725	60-53.214 S	55-57.238 W	762	3/5/2014	7/14/2014	135
Antarc_SSI_01	725	61-27.469 S	57-56.515 W	768	2/10/2015	1/29/2016	354
GofAK_AB_01	812	57-30.820 N	146-30.050 W	1200 ^a	4/29/2017	9/14/2017	138
GofAK_CA_04	719	59-00.609 N	148-53.963 W	203	9/6/2013	4/28/2014	235
GofAK_CA_05	707	59-00.500 N	148-54.100 W	201	4/29/2014	9/9/2014	133
GofAK_CB_01	626	58-38.741 N	148-04.129 W	1000	7/13/2011	2/19/2012	221
GofAK_CB_03	707	58-40.409 N	148-00.546 W	877	6/6/2013	9/5/2013	91
GofAK_CB_04	678	58-40.312 N	148-01.313 W	858	9/5/2013	4/28/2014	236
GofAK_CB_05	709	58-40.260 N	148-01.430 W	914	4/29/2014	9/9/2014	133
GofAK_CB_06	711	58-40.249 N	148-01.464 W	900	9/9/2014	5/2/2015	235
GofAK_CB_07	742	58-39.315 N	148-05.476 W	931	5/1/2015	9/6/2015	128
GofAK_CB_08	823	58-40.170 N	148-01.500 W	874	4/30/2017	9/12/2017	135
GofAK_CB_09	822	58-40.220 N	148-01.620 W	900	9/14/2017	6/16/2018	275
GofAK_KO_02	720	57-20.137 N	150-41.989 W	230	9/8/2013	5/1/2014	235
GofAK_KO_03	719	57-20.000 N	150-40.070 W	232	5/1/2014	9/11/2014	134
GofAK_PT_02	648	56-14.635 N	142-45.431 W	987	6/11/2013	8/20/2013	40
GofAK_PT_03	717	56-14.575 N	142-45.409 W	988	9/3/2013	3/21/2014	199
GofAK_PT_01	671	56-14.607 N	142-45.439 W	989	9/9/2012	6/10/2013	274
GofAK_QN_01	692	56-20.341 N	145-11.183 W	930	6/10/2013	9/11/2013	93
GofAK_QN_04	709	56-20.478 N	145-10.994 W	900	9/10/2014	5/2/2015	234
GofAK_QN_05	683	56-20.441 N	145-11.110 W	945	5/2/2015	8/18/2015	109
GofAK_QN_02	667	56-20.363 N	145-11.235 W	930	9/11/2013	4/16/2014	217
GofCA_CB_11	589	29-01.652 N	113-22.527 W	600	12/7/2009	5/18/2010	162
GofMX_DC_03	602	29-03.210 N	86-05.800 W	260	3/21/2011	7/6/2011	107
GofMX_DC_05	585	29-02.882 N	86-05.839 W	260	3/3/2012	12/9/2012	282

TABLE V. *Continued*

Data_ID	Hyd number	Latitude	Longitude	Depth (m)	Data_start	Data_end	Rec_Dur (days)
GofMX_DC_10	822	29-02.865 N	86-05.875 W	265	8/25/2016	7/18/2017	327
GofMX_DC_11	869	29-02.865 N	86-05.899 W	269	7/17/2017	6/9/2018	327
GofMX_DT_01	589	25-31.911 N	84-38.251 W	1320	8/9/2010	10/26/2010	79
GofMX_DT_02	589	25-31.911 N	84-38.251 W	1320	3/4/2011	6/24/2011	111
GofMX_DT_03	589	25-31.859 N	84-38.262 W	1300	7/13/2011	11/14/2011	124
GofMX_DT_09	715	25-32.316 N	84-37.878 W	1240	8/2/2015	3/15/2016	226
GofMX_DT_10	807	25-32.360 N	84-37.743 W	1210	6/22/2016	7/18/2017	392
GofMX_DT_11	868	25-32.355 N	84-37.733 W	1190	7/17/2017	6/27/2018	346
GofMX_GC_01	601	27-33.470 N	91-10.010 W	1115	7/15/2010	10/11/2010	88
GofMX_GC_02	601	27-33.466 N	91-10.014 W	1160	11/8/2010	2/2/2011	86
GofMX_GC_03	601	27-33.424 N	91-10.073 W	1100	3/23/2011	8/8/2011	138
GofMX_GC_04	601	27-33.426 N	91-10.060 W	1100	9/23/2011	2/17/2012	118
GofMX_GC_05	656	27-33.440 N	91-10.562 W	1100	2/28/2012	12/12/2012	289
GofMX_GC_06	694	27-33.347 N	91-10.092 W	1100	12/13/2012	9/10/2013	271
GofMX_GC_07	694	27-33.347 N	91-10.092 W	1100	1/13/2014	9/29/2014	254
GofMX_GC_08	719	27-33.366 N	91-10.073 W	1100	10/19/2014	6/10/2015	234
GofMX_GC_09	718	27-33.364 N	91-10.096 W	1133	8/7/2015	5/23/2016	289
GofMX_GC_10	809	27-33.367 N	91-10.083 W	1129	7/20/2016	5/17/2017	301
GofMX_GC_11	717	27-33.413 N	91-10.339 W	1100	5/16/2017	5/1/2018	351
GofMX_HH_01	560	25-01.702 N	84-23.769 W	1050	5/27/2012	12/6/2012	194
GofMX_HH_04	560	25-01.149 N	84-23.401 W	1067	9/28/2014	7/14/2015	289
GofMX_MC1_01	585	28-50.746 N	88-27.927 W	980	5/16/2010	8/28/2010	104
GofMX_MC1_02	585	28-50.771 N	88-27.907 W	980	9/7/2010	12/19/2010	103
GofMX_MC1_03	585	28-50.775 N	88-27.909 W	980	12/20/2010	3/21/2011	91
GofMX_MC1_05	585	28-50.797 N	88-27.991 W	980	9/22/2011	2/21/2012	152
GofMX_MC1_06	651	28-50.853 N	88-28.041 W	980	2/28/2012	12/11/2012	288
GofMX_MC1_13	728	28-50.832 N	88-27.973 W	990	5/17/2017	3/14/2018	301
GofMX_MC2_09	729	28-58.850 N	88-28.101 W	800	4/23/2014	9/28/2014	159
GofMX_MC2_10	718	28-58.732 N	88-28.082 W	800	9/29/2014	7/15/2015	289
GofMX_MP_01	578	29-15.204 N	88-17.753 W	86	7/4/2010	9/25/2010	83
GofMX_MP_03	596	29-15.318 N	88-17.808 W	93	3/23/2011	9/6/2011	167
GofMX_MP_04	596	29-15.354 N	88-17.702 W	93	9/22/2011	3/1/2012	161
GofMX_MP_05	652	29-15.368 N	88-17.597 W	90	2/29/2012	11/24/2012	270
GofMX_MP_06	683	29-15.379 N	88-17.514 W	90	12/10/2012	9/25/2013	289
GofMX_MP_08	729	29-15.177 N	88-17.590 W	100	10/2/2014	5/7/2015	217
GofMX_MP_09	719	29-15.115 N	88-17.506 W	90	8/9/2015	5/4/2016	269
GofMX_MP_11	731	29-15.145 N	88-17.356 W	120	5/17/2017	5/29/2018	378
Hawaii_EquatorA_01	564	00-26.607 N	164-08.079 W	1266	3/6/2012	6/17/2012	103
Hawaii_HowlandA_01	675	00-49.032 N	176-64.488 W	780	4/20/2017	1/28/2018	283
Hawaii_KauaiA_01	564	21-57.164 N	159-53.238 W	706	10/8/2009	5/13/2010	218
Hawaii_KauaiA_02	593	21-57.224 N	159-53.383 W	720	6/4/2010	8/20/2010	78
Hawaii_KauaiA_05	736	21-56.952 N	159-53.273 W	717	7/9/2016	8/9/2017	396
Hawaii_KingA_01	593	06-21.908 N	162-17.539 W	859	10/20/2011	3/11/2012	144
Hawaii_PaganA_01	695	17-57.785 N	145-28.867 E	830	5/25/2015	4/11/2017	688
Hawaii_PHRA_02	595	27-43.620 N	175-37.946 W	752	6/1/2010	9/17/2010	108
Hawaii_PHRA_04	593	27-43.519 N	175-38.257 W	550	4/12/2011	7/29/2011	108
Hawaii_PHRA_05	591	27-43.521 N	175-38.250 W	750	8/15/2011	1/7/2012	146
Hawaii_PHRA_08	716	27-44.462 N	175-33.588 W	985	9/12/2014	7/16/2015	308
Hawaii_PHRA_09	675	27-44.459 N	175-33.627 W	915	10/15/2015	8/14/2016	304
Hawaii_PHRA_10	678	27-44.459 N	175-33.627 W	915	8/20/2016	3/14/2017	207
Hawaii_PHRA_01	487	27-43.517 N	175-38.287 W	753	10/20/2009	5/24/2010	217
Hawaii_SaipanA_01	594	15-18.998 N	145-27.542 E	689	3/5/2010	8/25/2010	203
Hawaii_SaipanA_02	594	15-19.026 N	145-27.463 E	696	4/27/2011	10/20/2011	177
Hawaii_SaipanA_03	583	15-19.067 N	145-27.421 E	696	6/20/2012	3/8/2013	261
Hawaii_SaipanA_04	651	15-19.275 N	145-27.260 E	600	7/23/2013	1/17/2014	179
Hawaii_SaipanA_05	695	15-19.275 N	145-27.260 E	600	6/18/2014	4/17/2015	304
Hawaii_SaipanA_08	863	15-19.021 N	145-27.443 E	329	5/29/2017	6/2/2018	369
Hawaii_SaipanA06	668	15-19.046 N	145-27.433 E	696	5/13/2015	5/2/2016	356

TABLE V. *Continued*

Data_ID	Hyd number	Latitude	Longitude	Depth (m)	Data_start	Data_end	Rec_Dur (days)
Hawaii_TinianA_02	583	15-02.344 N	145-45.130 E	995	4/13/2011	11/22/2011	224
Hawaii_TinianA_03	598	15-02.388 N	145-45.319 E	1000	6/23/2012	5/14/2013	327
Hawaii_TinianA_04	695	15-02.241 N	145-45.228 E	1000	7/23/2013	6/15/2014	327
Hawaii_TinianA_05	651	15-02.241 N	145-45.228 E	1000	6/16/2014	11/11/2014	148
Hawaii_TinianA_07	668	15.02.241 N	145-45.228 E	1000	5/30/2016	11/5/2016	160
Hawaii_WakeS_01	593	19-13.200 N	166-41.005 E	800	1/31/2010	5/4/2010	93
Hawaii_WakeS_04	599	19-13.294 N	166-41.563 E	935	2/25/2012	1/3/2013	314
Hawaii_WakeS_05	730	19-13.330 N	166-41.673 E	849	6/20/2014	5/8/2015	381
Hawaii_WakeS_06	678	19-13.408 N	166-41.671 E	620	5/5/2015	5/24/2016	386
Hawaii_WakeS_07	651	19-22.324 N	166-69.378 E	620	4/12/2016	12/16/2016	248
OCNMS_CE_13	614	47-21.117 N	124-43.256 W	118	5/21/2011	11/6/2011	169
OCNMS_CE_14	587	47-21.141 N	124-43.275 W	150	12/7/2011	1/17/2012	42
OCNMS_QC_12	587	47-30.003 N	125-21.203 W	1394	1/27/2011	10/7/2011	253
OCNMS_QC_14	614	47-30.026 N	125-21.212 W	1394	12/7/2011	7/11/2012	218
OCNMS_QC_15	678	47-30.032 N	125-21.215 W	1394	9/14/2012	6/30/2013	289
Socal_A_19	425	33-15.039 N	118-14.963 W	318	10/22/2007	12/15/2007	55
Socal_A_22	429	33-15.107 N	118-14.897 W	308	12/13/2007	12/24/2007	12
Socal_A2_32	400	33-13.679 N	118-16.554 W	1141	3/10/2009	5/4/2009	55
Socal_B_32	412	34-16.528 N	120-01.129 W	577	2/12/2009	5/6/2009	55
Socal_BajaGL_01	860	29-08.462 N	118-15.658 W	1113	11/19/2018	10/22/2019	338
Socal_C_32	413	34-18.885 N	120-48.367 W	802	3/12/2009	5/5/2009	55
Socal_CCE1SB_01	818	33-28.970 N	122-34.560 W	812	10/10/2016	11/8/2017	395
Socal_CINMSB_02	451	34-16.584 N	120-01.512 W	610	4/17/2008	6/6/2008	51
Socal_CINMSB_03	472	34-16.621 N	120-01.661 W	580	7/23/2008	10/1/2008	71
Socal_CINMSB_04	471	34-16.617 N	120-01.492 W	576	10/16/2008	12/3/2008	49
Socal_CINMSB_05	472	34-16.528 N	120-01.132 W	580	12/4/2008	2/21/2009	80
Socal_CINMSB_09	412	34-16.732 N	120-01.664 W	580	9/3/2009	10/27/2009	54
Socal_CINMSB_12	580	34-16.704 N	120-01.620 W	581	3/2/2010	6/11/2010	101
Socal_CINMSB_13	581	34-16.968 N	120-01.684 W	549	6/25/2010	9/19/2010	86
Socal_CINMSB_16	580	34-16.991 N	120-01.697 W	580	4/6/2011	7/10/2011	92
Socal_CINMSB_17	646	34-16.970 N	120-01.706 W	580	10/27/2011	3/19/2012	144
Socal_CINMSB_18	618	34-17.126 N	120-01.632 W	580	3/24/2012	7/26/2012	125
Socal_CINMSB_19	672	34-17.156 N	120-01.473 W	900	8/2/2012	12/3/2012	124
Socal_CINMSB_20	695	34-17.131 N	120-01.636 W	900	12/16/2012	5/2/2013	138
Socal_CINMSB_21	691	34-17.112 N	120-01.640 W	580	5/2/2013	9/20/2013	140
Socal_CINMSB_22	725	34-17.115 N	120-01.639 W	535	9/21/2013	1/8/2014	110
Socal_CINMSB_27	714	34-17.168 N	120-01.717 W	600	2/6/2015	6/10/2015	125
Socal_CINMSB_29	780	34-17.105 N	120-01.666 W	579	10/5/2015	12/16/2015	72
Socal_CINMSB_30_00	780	34-16.532 N	120-01.112 W	585	12/16/2015	5/29/2016	165
Socal_CINMSB_31	738	34-17.095 N	120-01.630 W	578	7/27/2016	11/9/2016	105
Socal_CINMSC_04	472	34-19.110 N	120-48.333 W	700	10/15/2008	12/4/2008	51
Socal_CINMSC_05	413	34-18.902 N	120-48.370 W	700	12/3/2008	2/28/2009	88
Socal_CINMSC_10	581	34-19.108 N	120-48.465 W	780	11/4/2009	2/20/2010	102
Socal_CINMSC_12	581	34-19.097 N	120-48.445 W	801	3/3/2010	6/13/2010	102
Socal_CINMSC_13	580	34-19.000 N	120-48.410 W	915	6/24/2010	9/21/2010	89
Socal_CINMSC_15	580	34-18.997 N	120-48.412 W	850	11/16/2010	3/2/2011	107
Socal_CINMSC_16	581	34-19.007 N	120-48.349 W	850	4/5/2011	7/11/2011	94
Socal_CINMSC_18	645	34-19.500 N	120-48.400 W	758	3/25/2012	8/2/2012	131
Socal_CINMSC_20	692	34-19.020 N	120-48.336 W	800	12/18/2012	4/28/2013	132
Socal_CINMSC_23	692	34-18.973 N	120-48.295 W	828	1/14/2014	4/9/2014	85
Socal_CINMSC_26	762	34-19.474 N	120-48.474 W	600	11/4/2014	2/5/2015	93
Socal_CINMSC_28	762	34-19.562 N	120-48.405 W	754	6/11/2015	10/4/2015	116
Socal_CINMSC_32	762	34-19.455 N	120-48.426 W	760	11/10/2016	2/22/2017	104
Socal_DCPPC_01	682	35-24.000 N	121-33.750 W	1000	11/7/2012	3/19/2013	132
Socal_E_19	406	32-39.412 N	119-28.412 W	1288	10/23/2007	3/23/2008	152
Socal_E_27	453	32-39.448 N	119-28.288 W	1300	8/3/2008	9/26/2008	54
Socal_E_29	452	32-39.440 N	119-28.252 W	1295	10/19/2008	12/12/2008	55
Socal_E_31	477	32-39.427 N	119-28.430 W	1317	1/13/2009	3/9/2009	55

TABLE V. *Continued*

Data_ID	Hyd number	Latitude	Longitude	Depth (m)	Data_start	Data_end	Rec_Dur (days)
Socal_E_32	452	32-39.409 N	119-28.419 W	1308	3/13/2009	5/7/2009	55
Socal_E_33	481	32-39.379 N	119-28.389 W	1313	5/19/2009	7/12/2009	55
Socal_E_61	830	32-39.535 N	119-28.710 W	1331	3/5/2017	7/10/2017	128
Socal_E_62	830	32-39.538 N	119-28.812 W	1312	7/11/2017	2/10/2018	215
Socal_E_64	876	32-39.453 N	119-28.564 W	1300	7/12/2018	11/28/2018	140
Socal_G_18	405	32-55.605 N	118-37.254 W	480	7/23/2007	9/15/2007	55
Socal_G_19	413	32-55.602 N	118-37.248 W	471	10/22/2007	12/15/2007	55
Socal_G_26	454	32-55.639 N	118-37.105 W	435	6/4/2008	7/28/2008	55
Socal_G_32	426	32-55.619 N	118-38.135 W	458	1/13/2008	5/25/2008	133
Socal_G2_31	481	33-08.407 N	118-52.815 W	1130	1/13/2009	3/4/2009	50
Socal_G2_32	480	33-08.408 N	118-52.811 W	1126	3/10/2009	5/4/2009	56
Socal_G2_33	400	33-08.411 N	118-52.832 W	1126	5/16/2009	7/9/2009	54
Socal_G2_34	481	33-08.559 N	118-53.588 W	1106	7/26/2009	9/18/2009	54
Socal_G2_35	452	33-08.566 N	118-53.597 W	1108	9/25/2009	11/16/2009	56
Socal_H_18	407	32-50.813 N	119-10.600 W	1013	7/24/2007	9/16/2007	55
Socal_H_26	426	32-50.823 N	119-10.606 W	1012	6/5/2008	7/25/2008	51
Socal_H_27	452	32-50.841 N	119-10.489 W	1018	8/4/2008	9/27/2008	54
Socal_H_29	453	32-50.823 N	119-10.624 W	1015	10/21/2008	12/14/2008	55
Socal_H_30	478	32-50.754 N	119-10.387 W	1010	12/21/2008	1/12/2009	23
Socal_H_31	482	32-50.587 N	119-10.170 W	1004	1/13/2009	3/8/2009	55
Socal_H_32	477	32-50.587 N	119-10.170 W	935	3/14/2009	5/7/2009	55
Socal_H_34	560	32-50.569 N	119-10.294 W	992	7/23/2009	9/15/2009	54
Socal_H_35	481	32-50.564 N	119-10.279 W	995	9/25/2009	11/18/2009	55
Socal_H_37	566	32-50.554 N	119-10.272 W	992	1/30/2010	3/22/2010	52
Socal_H_40	591	32-50.552 N	119-10.254 W	1004	7/23/2010	11/8/2010	108
Socal_H_41	614	32-50.553 N	119-10.247 W	1002	12/6/2010	4/17/2011	133
Socal_H_44	618	32-50.558 N	119-10.287 W	989	5/11/2011	10/12/2011	123
Socal_H_45	649	32-50.537 N	119-10.217 W	1008	10/16/2011	3/5/2012	126
Socal_H_50	723	32-50.307 N	119-10.006 W	1000	9/10/2013	1/7/2014	118
Socal_H_51	729	32-50.307 N	119-10.006 W	960	1/7/2014	4/3/2014	87
Socal_H_52	740	32-50.800 N	119-10.588 W	986	4/4/2014	7/30/2014	117
Socal_H_55	734	32-50.778 N	119-10.584 W	1000	2/5/2015	6/1/2015	117
Socal_H_56	711	32-50.777 N	119-10.569 W	1000	6/2/2015	10/3/2015	123
Socal_H_58	711	32-50.749 N	119-10.620 W	1000	11/21/2015	4/25/2016	156
Socal_H_59	700	32-50.703 N	119-10.583 W	1000	7/6/2016	11/9/2016	126
Socal_H_61	844	32-50.752 N	119-10.523 W	1000	2/22/2017	6/6/2017	105
Socal_H_63	813	32-50.728 N	119-10.484 W	1000	10/5/2017	2/2/2018	121
Socal_H_65	815	32-50.536 N	119-10.249 W	1000	7/9/2018	11/29/2018	142
Socal_H_66	876	32-50.509 N	119-10.023 W	1013	11/29/2018	5/5/2019	158
Socal_M_31	452	33-30.582 N	119-15.282 W	895	1/13/2009	3/8/2009	55
Socal_M_32	481	33-30.579 N	119-15.280 W	1123	3/11/2009	5/4/2009	54
Socal_M_33	480	33-30.580 N	119-15.253 W	1120	5/17/2009	7/8/2009	52
Socal_M_34	452	33-30.927 N	119-14.794 W	902	7/27/2009	9/16/2009	51
Socal_M_35	578	33-30.923 N	119-14.779 W	912	9/25/2009	11/17/2009	53
Socal_M_37	473	33-30.915 N	119-14.960 W	891	1/30/2010	3/25/2010	54
Socal_M_38	596	33-30.897 N	119-14.896 W	917	4/10/2010	7/12/2010	93
Socal_M_40	588	33-30.891 N	119-14.832 W	909	7/22/2010	11/7/2010	108
Socal_M_41	618	33-30.897 N	119-14.888 W	919	12/5/2010	4/24/2011	140
Socal_M_44	560	33-30.887 N	119-14.875 W	928	5/11/2011	10/2/2011	113
Socal_M_45	618	33-30.886 N	119-14.886 W	927	10/27/2011	3/18/2012	143
Socal_M_46	662	33-30.826 N	119-14.880 W	926	3/24/2012	7/22/2012	121
Socal_M_48	691	33-30.599 N	119-15.305 W	907	12/20/2012	4/25/2013	127
Socal_M_49	700	33-30.607 N	119-15.305 W	882	4/30/2013	9/5/2013	127
Socal_M_50	724	33-30.584 N	119-15.252 W	907	9/10/2013	1/6/2014	119
Socal_M_52	736	33-30.595 N	119-15.305 W	890	4/4/2014	7/6/2014	93
Socal_M-51	731	33-30.577 N	119-15.251 W	877	1/6/2014	4/4/2014	88
Socal_N_31	478	32-22.204 N	118-33.908 W	1369	1/14/2009	3/9/2009	54
Socal_N_32	482	32-22.205 N	118-33.905 W	1295	3/14/2009	5/7/2009	55

TABLE V. *Continued*

Data_ID	Hyd number	Latitude	Longitude	Depth (m)	Data_start	Data_end	Rec_Dur (days)
Socal_N_33	452	32-22.197 N	118-33.893 W	1295	5/19/2009	7/12/2009	54
Socal_N_34	561	32-22.186 N	118-33.885 W	1287	7/22/2009	9/15/2009	55
Socal_N_35	560	32-22.191 N	118-33.887 W	1295	9/26/2009	11/19/2009	54
Socal_N_36	585	32-22.186 N	118-33.769 W	1282	12/6/2009	1/26/2010	51
Socal_N_37	587	32-22.184 N	118-33.768 W	1280	1/31/2010	3/26/2010	54
Socal_N_38	566	32-22.180 N	118-33.800 W	1284	4/11/2010	7/18/2010	98
Socal_N_40	584	32-22.182 N	118-33.803 W	1288	7/23/2010	11/8/2010	108
Socal_N_41	591	32-22.183 N	118-33.802 W	1271	12/7/2010	4/9/2011	123
Socal_N_45	643	32-22.199 N	118-33.894 W	1295	10/16/2011	2/13/2012	121
Socal_N_46	643	32-22.200 N	118-33.903 W	1292	3/25/2012	8/5/2012	134
Socal_N_47	668	32-22.157 N	118-33.938 W	1285	8/10/2012	12/6/2012	119
Socal_N_49	672	32-22.194 N	118-33.892 W	1292	5/2/2013	9/11/2013	131
Socal_N_52	738	32-22.197 N	118-33.913 W	1154	4/4/2014	7/30/2014	117
Socal_N_53	740	32-22.185 N	118-33.820 W	1260	7/30/2014	11/5/2014	98
Socal_N_55	736	32-22.211 N	118-33.937 W	1000	2/5/2015	6/1/2015	117
Socal_N_56	706	32-22.223 N	118-33.841 W	1260	6/2/2015	10/3/2015	124
Socal_N_57	724	32-22.212 N	118-33.871 W	1260	10/3/2015	11/21/2015	49
Socal_N_59	742	32-22.251 N	118-33.863 W	1200	7/7/2016	11/8/2016	125
Socal_N_62	809	32-22.248 N	118-33.852 W	1300	6/7/2017	12/21/2017	197
Socal_N_63	815	32-22.230 N	118-33.872 W	1296	2/4/2018	7/9/2018	155
Socal_N_64	809	32-22.137 N	118-33.874 W	1290	7/9/2018	11/28/2018	142
Socal_N_61	857	32-22.256 N	118-33.884 W	1300	2/21/2017	6/7/2017	105
Socal_P_36	588	32-53.598 N	117-22.714 W	477	12/4/2009	1/12/2010	39
Socal_PSA_12	641	36-17.945 N	122-23.633 W	1412	11/30/2011	6/24/2012	207
Socal_PSB_07	486	36-23.336 N	122-18.409 W	847	5/1/2009	9/22/2009	144.2
Socal_PSB_09	486	36-23.479 N	122-18.450 W	837	2/26/2010	11/3/2010	250
Socal_PSB_11	627	36-23.472 N	122-18.419 W	850	6/21/2011	4/7/2012	291
Socal_Q_35	566	33-49.222 N	118-37.775 W	682	9/24/2009	11/17/2009	55
Socal_Q_36	584	33-49.204 N	118-37.762 W	687	12/4/2009	1/25/2010	52
Socal_Q_38	588	33-49.209 N	118-37.681 W	671	4/9/2010	7/21/2010	103
Socal_R_36	578	33-09.628 N	120-00.615 W	1200	12/8/2009	1/28/2010	51
Socal_R_37	584	33-09.621 N	120-00.606 W	1188	1/30/2010	3/25/2010	54
Socal_R_38	591	33-09.601 N	120-00.522 W	1202	4/10/2010	7/20/2010	47
Socal_R_40	596	33-09.599 N	120-00.499 W	1197	7/22/2010	10/25/2010	95
Socal_S_37	585	32-29.092 N	118-16.370 W	1375	1/31/2010	3/20/2010	48
Socal_S_38	587	32-29.092 N	118-16.309 W	1380	4/11/2010	7/10/2010	90
Socal_S_40	566	32-29.096 N	118-16.293 W	1388	7/23/2010	8/18/2010	27
Socal_S_41	566	32-29.102 N	118-16.323 W	1380	12/7/2010	5/1/2011	145
Socal_SN_40	611	32-54.897 N	120-22.523 W	1086	7/22/2010	11/6/2010	107
Socal_SN_56	731	32-54.945 N	120-22.558 W	1289	6/11/2015	10/2/2015	113
Socal_SN_57	731	32-54.917 N	120-22.519 W	1090	3/17/2016	1/7/2017	296
Socal_SN_58	738	32-54.936 N	120-22.544 W	1090	3/5/2017	9/10/2017	190
Socal_SN_59	738	32-54.771 N	120-22.445 W	1090	10/4/2017	8/2/2018	301
Socal_T_02	700	32-53.212 N	117-33.362 W	825	3/5/2017	7/6/2017	124
Socal_T_03	700	32-53.199 N	117-33.496 W	814	7/8/2017	1/18/2018	195
Socal_TB_01	823	32-53.914 N	117-36.586 W	900	9/29/2016	12/15/16	78
Socal_U_01	856	31-51.098 N	118-29.071 W	1200	11/17/2018	6/11/2019	206
WAT_BC_01	814	39-11.463 N	72-13.722 W	1000	4/20/2016	6/10/2017	416
WAT_BC_02	876	39-11.430 N	72-13.628 W	1000	6/30/2017	6/3/2018	338
WAT_BC_03	802	39-11.515 N	72-13.641 W	997	6/3/2018	5/19/2019	350
WAT_BMA_01	709	31-55.575 N	65-12.900 W	713	6/10/2013	3/11/2014	274
WAT_BMA_03	723	31-55.415 N	65-12.113 W	732	12/17/2014	10/2/2015	289
WAT_BP_01	810	32-06.362 N	77-05.659 W	945	4/28/2016	6/27/2017	425
WAT_BP_02	844	32-06.417 N	77-05.406 W	941	6/27/2017	6/28/2018	366
WAT_BS_01	815	30-35.027 N	77-23.443 W	1005	4/27/2016	6/26/2017	425
WAT_BS_02	879	30-34.982 N	77-23.426 W	1005	6/26/2017	6/23/2018	362
WAT_BS_03	841	30-34.977 N	77-23.401 W	1000	6/28/2018	6/16/2019	354
WAT_GS_01	813	33-39.938 N	76-00.083 W	953	4/29/2016	6/27/2017	425

TABLE V. *Continued*

Data_ID	Hyd number	Latitude	Longitude	Depth (m)	Data_start	Data_end	Rec_Dur (days)
WAT_GS_02	878	33-40.021 N	75-59.968 W	930	6/28/2017	6/26/2018	364
WAT_GS_03	844	33-40.195 N	75-59.862 W	940	6/28/2018	6/18/2019	354
WAT_HATA_01	561	35-20.432 N	74-51.457 W	950	3/15/2012	4/11/2012	26
WAT_HATA_05	700	35-20.531 N	74-51.436 W	980	4/7/2015	1/21/2016	290
WAT_HATA_06	816	35-18.110 N	74-52.737 W	1021	4/29/2016	2/6/2017	283
WAT_HATA03	667	35-20.667 N	74-51.126 W	970	5/29/2013	3/15/2014	289
WAT_HATB_04_01	807	35-35.386 N	74-44.856 W	1350	6/1/2018	12/14/2018	196
WAT_HATB_05	815	35-35.358 N	74-45.270 W	1175	12/14/2018	5/17/2019	155
WAT_HZ_01	734	41-03.715 N	66-21.092 W	845	6/27/2015	3/25/2016	271
WAT_HZ_03	865	41-03.699 N	66-21.093 W	1090	7/9/2017	1/13/2018	189
WAT_HZ_04	810	41-03.699 N	66-21.093 W	1090	6/11/2018	5/10/2019	333
WAT_JAX_D_13	808	30-09.110 N	79-46.213 W	736	4/26/2016	6/25/2017	425
WAT_JAXA_02	478	30-16.831 N	80-12.962 W	83	9/16/2009	12/27/2009	102
WAT_JAXA_03	471	30-16-520 N	80-12.551 W	89	2/22/2010	7/30/2010	158
WAT_JAXB_01	478	30-15.492 N	80-25.692 W	37	4/2/2009	9/5/2009	156
WAT_JAXC_10	673	30-19.586 N	80-12.296 W	88	2/17/2014	8/23/2014	187
WAT_JAXD_11	681	30-09.036 N	79-46.203 W	800	8/23/2014	5/29/2015	279
WAT_JAXD_15	823	30-09.135 N	79-46.236 W	740	6/27/2018	6/15/2019	354
WAT_NC_01	740	39-49.949 N	69-58.928 W	977	4/27/2015	9/18/2015	145
WAT_NC_02	811	39-49.943 N	69-58.926 W	977	4/21/2016	5/24/2017	398
WAT_NC_04	811	39-49.977 N	69-58.916 W	977	6/10/2018	6/3/2019	358
WAT_NFCA_02	814	37-09.991 N	74-27.996 W	968	4/30/2016	6/28/2017	424
WAT_NFCA_03	877	37-10.044 N	74-27.980 W	950	6/30/2017	6/2/2018	337
WAT_NFCA_04	808	37-09.871 N	74-27.951 W	1050	6/2/2018	5/18/2019	350
WAT_OC_01	707	40-15.798 N	67-59.174 W	1100	4/26/2015	2/9/2016	289
WAT_OC_04	816	40-13.800 N	67-58.679 W	790	6/10/2018	5/19/2019	343
WAT_USWTRA_01	412	33-47.483 N	76-31.429 W	162	10/10/2007	1/16/2008	99
WAT_USWTRC_04	561	33-40.670 N	76-28.613 W	335	11/8/2009	4/20/2009	163
WAT_USWTRD_05	561	33-34.839 N	76-33.009 W	338	7/30/2010	2/4/2011	190
WAT_WC_01	802	38-22.449 N	73-22.241 W	1000	4/20/2016	6/29/2017	436
WAT_WC_02	816	38-22.431 N	73-22.209 W	1000	6/30/2017	6/2/2018	338
WAT_WC_03	820	38-22.402 N	73-22.191 W	974	6/2/2018	5/19/2019	350

^aSensor depth.

TABLE VI. Hydrophone specifications including low and high frequency sensors, crossover frequency, and sensitivity.

ID	Low frequency sensor	High frequency sensor	Cross over frequency (kHz)	Sensitivity @ 1 KHz (dB: re V/uPa)	Sensitivity @ 10 KHz (dB: re V/uPa)
400	6 × AQ-1	ITC 1042	2	-156	-129
500	6 × AQ-1	ITC 1042	3	-155	-154
600	6 × AQ-1	ITC 1042	3	-154	-154
700	6 × AQ-1	ITC 1042	20	-153	-156
800	ITC 1042	ITC 1042	None	-150	-151

¹See supplementary material at <https://www.scitation.org/doi/suppl/10.1121/10.0005430> for the ocean noise model of Ross (1954).

Ainslie, M., and McColm, J. (1998). "A simplified formula for viscous and chemical absorption in sea water," *J. Acoust. Soc. Am.* **103**, 1671–1672.
 Atlas, R., Hoffman, R. N., Ardizzone, J., Leidner, S. M., Jusem, J. C., Smith, D. K., and Gombos, D. (2011). "A cross-calibrated, multiplatform ocean surface wind velocity product for meteorological and oceanographic applications," *Bull. Am. Meteorol. Soc.* **92**, 157–174.
 Bourassa, M. A., Meissner, T., Cerovecki, I., Chang, P. S., Dong, X., De Chiara, G., Donlon, C., Dukhovskoy, D. S., Elya, J., Fore, A., Fewings,

M. R., Foster, R. C., Gille, S. T., Haus, B. K., Hristova-Veleva, S., Holbach, H. M., Jelenak, Z., Knaff, J. A., Kranz, S. A., Manaster, A., Mazloff, M., Mears, C., Mouche, A., Portabella, M., Reul, N., Ricciardulli, L., Rodriguez, E., Sampson, C., Solis, D., Stoffelen, A., Stukel, M. R., Stiles, B., Weissman, D., and Wentz, F. (2019). "Remotely sensed winds and wind stresses for marine forecasting and ocean modeling," *Front. Mar. Sci.* **6**, 443.
 Burgess, A. S., and Kewley, D. J. (1983). "Wind-generated surface noise source levels in deep water east of Australia," *J. Acoust. Soc. Am.* **73**, 201–210.
 Carey, W. M., and Browning, D. (1988). "Low frequency ocean ambient noise: Measurements and theory," in *Sea Surface Sound: Natural*

- Mechanisms of Surface Generated Noise in the Ocean*, edited by B. R. Kerman (Springer, Dordrecht, the Netherlands), pp. 361–376.
- Carey, W. B., and Evans, R. B. (2011). *Ocean Ambient Noise, Measurement and Theory* (Springer, New York).
- Cato, D. H. (1976). “Ambient sea noise in waters near Australia,” *J. Acoust. Soc. Am.* **60**, 320–328.
- Chapman, N. R., and Cornish, J. W. (1993). “Wind dependence of deep ocean ambient noise at low frequencies,” *J. Acoust. Soc. Am.* **93**, 782–789.
- Evans, D. L., Watts, D. R., Halpern, D., and Bourassa, S. (1984). “Oceanic winds measured from the seafloor,” *J. Geophys. Res. Oceans* **89**, 3457–3461, <https://doi.org/10.1029/JC089iC03p03457>.
- Farmer, D. M., and Lemon, D. D. (1984). “The influence of bubbles on ambient noise in the ocean at high wind speeds,” *J. Phys. Oceanogr.* **14**, 1762–1778.
- Farrokhrooz, M., Wage, K. E., Dzieciuch, M. A., and Worcester, P. F. (2017). “Vertical line array measurements of ambient noise in the North Pacific,” *J. Acoust. Soc. Am.* **141**, 1571–1581.
- Franz, G. J. (1959). “Splashes as Sources of Sound in Liquids,” *J. Acoust. Soc. Am.* **31**, 1080–1096.
- Gassmann, M., Wiggins, S. M., and Hildebrand, J. A. (2017). “Deep-water measurements of container ship radiated noise signatures and directionality,” *J. Acoust. Soc. Am.* **142**, 1563–1574.
- Gillot, G., Derec, C., Génevaux, J.-M., Simon, L., and Benyahia, L. (2020). “A new insight on a mechanism of airborne and underwater sound of a drop impacting a liquid surface,” *Phys. Fluids* **32**, 062004.
- Hildebrand, J. A. (2009). “Anthropogenic and natural sources of ambient noise in the ocean,” *Mar. Ecol. Prog. Ser.* **395**, 5–20.
- Ingenito, F., and Wolf, S. N. (1989). “Site dependence of wind-dominated ambient noise in shallow water,” *J. Acoust. Soc. Am.* **85**, 141–145.
- Kerman, B. R. (1984). “Underwater sound generation by breaking wind waves,” *J. Acoust. Soc. Am.* **75**, 149–165.
- Kewley, D. J., Browning, D. G., and Carey, W. M. (1990). “Low-frequency wind-generated ambient noise source levels,” *J. Acoust. Soc. Am.* **88**, 1894–1902.
- Kibblewhite, A. C., and Ewans, K. C. (1985). “Wave–wave interactions, microseisms, and infrasonic ambient noise in the ocean,” *J. Acoust. Soc. Am.* **78**, 981–994.
- Knudsen, V. O., Alford, R. S., and Emling, J. W. (1948). “Underwater ambient noise,” *J. Mar. Res.* **7**, 410–429.
- Kuperman, W. A., and Ingenito, F. (1980). “Spatial correlation of surface generated noise in a stratified ocean,” *J. Acoust. Soc. Am.* **67**, 1988–1996.
- Kurahashi, N., and Gratta, G. (2008). “Ocean ambient noise as a background to acoustic neutrino detection,” *Phys. Rev. D* **78**, 1–5.
- Loewen, M. R., and Melville, W. K. (1991). “A model of the sound generated by breaking waves,” *J. Acoust. Soc. Am.* **90**, 2075–2080.
- Ma, B. B., Nystuen, J. A., and Lien, R.-C. (2005). “Prediction of underwater sound levels from rain and wind,” *J. Acoust. Soc. Am.* **117**, 3555–3565.
- Marrett, R., and Chapman, N. R. (1990). “Low-frequency ambient-noise measurements in the South Fiji basin,” *IEEE J. Oceanic Eng.* **15**, 311–315.
- McDonald, M. A., Hildebrand, J. A., Wiggins, S. M., and Ross, D. (2008). “A 50 year comparison of ambient ocean noise near San Clemente Island: A bathymetrically complex coastal region off Southern California,” *J. Acoust. Soc. Am.* **124**, 1985–1992.
- McKenna, M. F., Ross, D., Wiggins, S. M., and Hildebrand, J. A. (2012). “Underwater radiated noise from modern commercial ships,” *J. Acoust. Soc. Am.* **131**, 92–103.
- Means, S. L., and Heitmeyer, R. M. (2001). “Low-frequency sound generation by an individual open-ocean breaking wave,” *J. Acoust. Soc. Am.* **110**, 761–768.
- Meissner, T., and Wentz, F. J. (2012). “The emissivity of the ocean surface between 6 and 90 GHz over a large range of wind speeds and earth incidence angles,” *IEEE Trans. Geosci. Remote Sens.* **50**, 3004–3026.
- Nystuen, J. A., Moore, S. E., and Stabenro, P. J. (2010). “A sound budget for the southeastern Bering Sea: Measuring wind, rainfall, shipping, and other sources of underwater sound,” *J. Acoust. Soc. Am.* **128**, 58–65.
- Perrone, A. J. (1969). “Deep-ocean ambient-noise spectra in the Northwest Atlantic,” *J. Acoust. Soc. Am.* **46**, 762–770.
- Piggott, C. L. (1964). “Ambient sea noise at low frequencies in shallow water of the Scotian Shelf,” *J. Acoust. Soc. Am.* **36**, 2152–2163.
- Prosperetti, A. (1988). “Bubble dynamics in oceanic ambient noise,” in *Sea Surface Sound: Natural Mechanisms of Surface Generated Noise in the Ocean*, edited by B. R. Kerman (Springer Dordrecht, the Netherlands), pp. 151–171.
- Pumphrey, H. C., and Elmore, P. A. (1990). “The entrainment of bubbles by drop impacts,” *J. Fluid Mech.* **220**, 539–567.
- Reeder, D. B., Sheffield, E. S., and Mach, S. M. (2011). “Wind-generated ambient noise in a topographically isolated basin: A pre-industrial era proxy,” *J. Acoust. Soc. Am.* **129**, 64–73.
- Ross, D. (1954). *Generalized Ambient Spectra* (Document Bell Telephone Laboratories, Holmdel, NJ).
- Ross, D. (1976). *Mechanics of Underwater Noise* (Pergamon Press, New York).
- Roth, E. H., Hildebrand, J. A., Wiggins, S. M., and Ross, D. (2012). “Underwater ambient noise on the Chukchi Sea continental slope from 2006–2009,” *J. Acoust. Soc. Am.* **131**, 104–110.
- Short, J. R. (2005). “High-frequency ambient noise and its impact on underwater tracking ranges,” *IEEE J. Oceanic Eng.* **30**, 267–274.
- Tkalich, P., and Chan, E. S. (2002). “Breaking wind waves as a source of ambient noise,” *J. Acoust. Soc. Am.* **112**, 456–463.
- Updegraff, G. E., and Anderson, V. C. (1991). “Bubble noise and wavelet spills recorded 1 m below the ocean surface,” *J. Acoust. Soc. Am.* **89**, 2264–2279.
- Urick, R. J. (1975). *Principles of Underwater Sound* (McGraw-Hill, New York).
- Urick, R. J. (1984). *Ambient Noise in the Sea* (Undersea Warfare Technology Office, Naval Sea Systems Command, Department of the Navy, Washington, DC).
- Webb, S. C. (1998). “Broadband seismology and noise under the ocean,” *Rev. Geophys.* **36**, 105–142, <https://doi.org/10.1029/97RG02287>.
- Wentz, F. J., Scott, J., Hoffman, R., Leidner, M., Atlas, R., and Ardizzone, J. (2016). “Cross-Calibrated Multi-Platform Ocean Surface Wind Vector Analysis Product V2, 1987—Ongoing,” Research Data Archive at the National Center for Atmospheric Research, Computational and Information Systems Laboratory, <https://doi.org/10.5065/4TSY-K140> (Last viewed October 1, 2020).
- Wenz, G. M. (1962). “Acoustic ambient noise in the ocean: Spectra and sources,” *J. Acoust. Soc. Am.* **34**, 1936–1956.
- Weston, D. E. (1989). “On the losses due to storm bubbles in oceanic sound transmission,” *J. Acoust. Soc. Am.* **86**, 1546–1553.
- Wiggins, S. M., Hall, J. M., Thayre, B. J., and Hildebrand, J. A. (2016). “Gulf of Mexico low-frequency ocean soundscape impacted by airguns,” *J. Acoust. Soc. Am.* **140**, 176–183.
- Wiggins, S. M., and Hildebrand, J. A. (2007). “High-frequency acoustic recording package (HARP) for broad-band, long-term marine mammal monitoring,” in *Proceedings of the 2007 Symposium on Underwater Technology and Workshop on Scientific Use of Submarine Cables and Related Technologies*, April 17–20, Tokyo, Japan, Document 551–557.
- Wiggins, S. M., and Hildebrand, J. A. (2012). “Monitoring cetaceans over long periods using autonomous acoustic recording packages,” in *Listening in the Ocean*, edited by W. W. Au (Springer-Verlag, Berlin, Germany).
- Wille, P. C., and Geyer, D. (1984). “Measurements on the origin of the wind-dependent ambient noise variability in shallow water,” *J. Acoust. Soc. Am.* **75**, 173–185.
- Wilson, J. H. (1979). “Very low frequency (VLF) wind-generated noise produced by turbulent pressure fluctuations in the atmosphere near the ocean surface,” *J. Acoust. Soc. Am.* **66**, 1499–1507.
- Wilson, J. H. (1980). “Low-frequency wind-generated noise produced by the impact of spray with the ocean’s surface,” *J. Acoust. Soc. Am.* **68**, 952–956.
- Wilson, J. H. (1983). “Wind-generated noise modeling,” *J. Acoust. Soc. Am.* **73**, 211–216.
- WMO (1970). “Beaufort scale of wind force (technical and operational aspects),” Commission for Marine Meteorology, Report on Marine Science Affairs No. 3, Document 22.
- Yen, N., and Perrone, A. J. (1979). “Mechanisms and modelling of wind-induced low frequency ambient sea noise,” Document NUSC Tech. Report No. 5833 (NUSC, London).